Rab8 directs furrow ingression and membrane addition during epithelial formation in *Drosophila melanogaster*

Lauren M. Mavor[1], Hui Miao[1], Zhongyuan Zuo[1], Ryan M. Holly[1], Yi Xie[1], Dinah Loerke[2], and J. Todd Blankenship[1]*

[1] Department of Biological Sciences, University of Denver, Denver, CO 80208, USA
[2] Department of Physics, University of Denver, Denver, CO 80208, USA
* Author for correspondence (email: todd.blankenship@du.edu; phone: (303) 871-3065; fax: (303) 871-3471)

Keywords: cellularization, Rab8, furrow formation

Abstract

One of the most fundamental changes in cell morphology is the ingression of a plasma membrane furrow. The *Drosophila* embryo undergoes several cycles of rapid furrow ingression during early development that culminates in the formation of an epithelial sheet. Previous studies have demonstrated the requirement for intracellular trafficking pathways in furrow ingression; however, the pathways that link compartmental behaviors with cortical furrow ingression events have remained unclear. Here, we show that Rab8 has striking dynamic behaviors *in vivo*. As furrows ingress, cytoplasmic Rab8 puncta are depleted and Rab8 accumulates at the plasma membrane in a location that coincides with known regions of directed membrane addition. We additionally use CRISPR/Cas9 technology to N-terminally tag Rab8, which is then used to address both endogenous localization and function. Endogenous Rab8 displays partial coincidence with Rab11 and the Golgi, and this colocalization is enriched during the fast phase of cellularization. When Rab8 function is disrupted, furrow formation in the early embryo is completely abolished. We also demonstrate that Rab8 behaviors require the function of the exocyst complex subunit Sec5 as well as the recycling endosome Rab11. Active, GTP-locked Rab8 is primarily associated with dynamic membrane compartments and the plasma membrane, while GDP-locked Rab8 forms large cytoplasmic aggregates. These studies suggest a model in which active Rab8 populations direct furrow ingression by guiding the targeted delivery of cytoplasmic membrane stores to the cell surface through exocyst tethering complex interactions.

Introduction

Ingression of a plasma membrane furrow is an essential cell shape change that occurs in all eukaryotic organisms. Furrow ingression is also an obligatory step in animal cells during cytokinesis. Understanding how cells are able to dynamically remodel plasma membrane topologies and form a stable furrow *in vivo* is an unresolved question. The early *Drosophila* embryo forms thousands of furrows, with some being generated in as little as four minutes (Holly et al., 2015). Fly embryos make both transient and permanent furrows in the course of development. Following fertilization and the fusion of the male and female pronuclei, the zygotic nucleus undergoes thirteen rounds of replication in the absence of cell division to generate a single-celled embryo with approximately 5,000 nuclei (Hartenstein, 1993). The first nine rounds of replication occur deep in the yolk of the embryo; however, at cycle 10, nuclei migrate to the periphery and begin organizing the formation of cytokinetic-like furrows that serve to separate mitotic nuclei in the syncytium. These furrows are transient, forming during each syncytial cycle where they compartmentalize and anchor mitotic spindles, before then regressing. Embryos undergo four rapid rounds of furrow formation (cycles 10-13), followed by a final fifth round of furrow ingression which results in the permanent packaging of nuclei into individual cells and the formation of an epithelium through a process known as cellularization.

Furrow ingression during cellularization shares mechanistic similarities to the earlier syncytial furrows and requires the function of filamentous actin (F-actin), microtubule, and membrane trafficking networks. A contractile actomyosin array directs the basal movement of a bulbous furrow canal, while new membrane delivery is targeted apically (reviewed in Schejter and Wieschaus, 1993; Mazumdar and Mazumdar, 2002; Lecuit, 2004). Microtubules are essential during the early, or slow phase, of cellularization and appear to provide the directional cue that orients the cellularization network (Foe et al., 2000). After the slow phase of cellularization, the network shifts into a fast phase of rapid furrow ingression and membrane addition is targeted to an apicolateral location (Lecuit and Wieschaus, 2000).

One puzzling aspect of furrow formation in the *Drosophila* embryo has been the absence of identified dynamic membrane compartment behaviors that are directed towards the furrow. The plasma membrane grows approximately 30-fold during

cellularization, and requires new membrane addition for its growth. While some furrow membrane is derived from the flattening of apical microvilli, both Golgi and recycling endosomal (RE) pathways have been shown to be required for furrow ingression, and membrane marking experiments have indicated regions where directed membrane addition is likely to occur (Lecuit and Wieschaus, 2000; Sisson et al., 2000; Pelissier et al., 2003; Riggs et al., 2003, Fabrowski et al., 2013; Figard et al., 2013). However, markers for Golgi and RE compartments, such as Lava Lamp and Rab11, do not display an association with, or move in a polarized fashion towards, the developing furrow (Sisson et al., 2000; Pelissier et al., 2003; Riggs et al., 2003).

The Rab family of small GTPase proteins are key mediators of membrane trafficking and cytoskeletal dynamics. When in an active GTP-bound state, Rab proteins regulate membrane compartment behaviors through their association with tethering and trafficking effectors (Pfeffer, 2005; Grosshans et al., 2006; Horgan and McCaffrey, 2012), and mutations in Rab proteins are associated with a variety of diseases and developmental disorders (Baskys et al., 2007; Mitra et al., 2011; Recchi and Seabra, 2012; Hardiman et al., 2012). At the plasma membrane Rab proteins have been shown to bind to the vesicular tethering exocyst complex. During lumen formation and ciliogenesis in mammalian cells, Rab8 binds to the Sec15 subunit of the exocyst complex (Bryant et al., 2010; Knödler et al., 2010; Feng at al., 2012), and the Rab11 recycling endosome protein can directly associate with the exocyst subunits Sec5 and Sec15 (Zhang et al., 2004; Beronja et al., 2005; Jafar-Nejad et al., 2005; Langevin et al., 2005; Wu et al., 2005). A newly emerging theme on Rab protein function is that Rab proteins and membrane trafficking pathways can also act through the cytoskeleton (Riggs et al., 2003; Hattula et al., 2006; Cao et al., 2008; Zhang et al., 2009; Peranen, 2011). A complete collection of YFP-tagged constitutively active and dominant negative, as well as wild type, lines of all known Drosophila Rab proteins has been constructed (Zhang et al., 2007), making it possible to screen for Rab proteins that are required for early embryonic development. An additional collection of large genomic fragment-driven Rab Gal4s permits the systematic profiling of the cellular and subcellular expression of Rab GTPases (Chan et al., 2011).

The Rab8 protein has been identified within the Rab family as associating with late exocytic vesicles. This protein has been demonstrated to direct polarized trafficking events during ciliogenesis, neuronal development, regulated secretion and cytokinesis (Yoshimura et al., 2007; Nachury et al., 2007; Huber et al., 1995; Chen et al., 2001; Kaplan and Reiner 2011), possibly through the ability to reorganize actin and microtubules (Peranen et al., 1996). Defects in Rab8 function have been implicated in trafficking diseases including retinal degeneration, cell polarity defects, and irregular tissue formation (Moritz et al., 2001; Satoh et al., 2007; Huber et al., 1995). Here, we show that Rab8 demonstrates dynamic behaviors that are specifically associated with furrow ingression in the early *Drosophila* embryo. Rab8 transitions from an intracellular punctate localization to an association with the apicolateral plasma membrane, and furrow ingression is abolished when Rab8 function is compromised. We also use CRISPR/Cas9 techniques to engineer a GFP:Rab8 fusion at the endogenous Rab8 locus. Our results suggest a model in which Rab8 cooperates with cytoplasmic Rab11 and Golgi stores to direct the targeted membrane delivery that is required for furrow ingression via interactions with the exocyst tethering complex.

Results

Rab8 exhibits dynamic behaviors in the early *Drosophila* embryo

We performed an initial screen to determine which of the *Drosophila* Rab proteins were involved in early developmental processes. Either GDP-dissociation deficient, dominant negative (DN) or GTPase deficient, constitutively active (CA) Rab proteins were expressed in embryos and scored under oil for tissue-level defects in early embryonic development (Supplemental Fig. 1). From this screen, we found that expression of Rab8 DN produce the strongest disruption of early embryogenesis and resulted in embryos with an uneven epithelium and a loss of later gastrulation movements (data not shown), suggesting that Rab8 is required in early morphological processes.

These results led us to examine the dynamics of Rab8 in early embryos. Embryos expressing YFP:Rab8 driven from a genomic Rab8-Gal4 were imaged using a spinning disc microscope. Prior to the movement of nuclei to the embryonic periphery at cycle 10, Rab8 exists in small, relatively static, puncta (Movie S1). However, once furrow formation is initiated in the syncytial divisions, Rab8 displays striking behaviors (Fig. 1A, Movie S2). As the syncytial cycle proceeds, Rab8 puncta become more numerous (Fig. 1A-A'). Rab8 then transitions to an association with the plasma membrane, and the cytoplasmic punctate population becomes depleted (Fig. 1A''). The association with the cell periphery is rapid and occurs within a few minutes (Fig. 1A-A"), which then persists through the remainder of the division cycle (Fig. 1A''').

To identify how changes in Rab8 populations are correlated with the cell cycle, we analyzed Rab8 localization in fixed embryos stained for YFP:Rab8 and DNA (Fig. 1B-E). During interphase of syncytial cycles 10-13, Rab8 exists in a punctate population (Fig. 1B), but then transitions to an association with the plasma membrane at the onset of prophase and mitosis (Fig. 1C). These structures persist through the mitotic division (Fig. 1D) and return to a punctate population at the onset of the next interphase (Fig. 1E). These results suggest that Rab8 behaviors are cell cycle regulated and undergo a transition from cytoplasmic membrane compartments to the cell periphery that correlates with the time period when syncytial furrow formation occurs.

Rab8 accumulation at the plasma membrane occurs during fast phase of cellularization

Similar to the earlier formation of syncytial furrows, Rab8 shows a transition from punctate structures to a hexagonal, cell periphery-associated array during cellularization. At early cellularization stages, Rab8 exists in punctate structures (Fig. 1F, Movie S3). As cellularization proceeds, these puncta become more numerous (Fig. 1F', G). Rab8 then makes a transition to a tight peripheral array (Fig. 1F"). The cytoplasmic puncta become depleted and the association with the plasma membrane persists throughout the remainder of cellularization (Fig. 1F"', G). This transition from punctate structures to a peripheral association also represents a transition from the slow phase (Fig. 2A,B) to the fast phase of cellularization (Fig. 2C,D), which is marked by the F-actin furrows reaching the basal-most portion of the nuclei (Fig. 2C). During fast phase, furrow ingression rapidly increases and membrane addition is targeted to an apicolateral location (Lecuit and Wieschaus, 2000). Rab8 localizes to this area of rapid membrane addition (Fig. 2C,D). Additionally, the similarity in Rab8 behavior during both syncytial divisions and cellularization suggests that both these processes may use Rab8-dependent machinery to initiate furrow formation.

In order to determine that the dynamics displayed in UASp-YFP:Rab8 embryos accurately reported the behaviors of endogenous Rab8 protein, we utilized CRISPR-HDR to insert eGFP into the genomic *Drosophila* Rab8 locus (Baena-Lopez et al., 2013; Bassett et al., 2013; Gratz et al., 2013; Gokcezade et al., 2014). To this end, a donor DNA consisting of the genomic DNA 1.5kb upstream (5') of the Rab8 ATG start site was cloned into the pBluescript KS plasmid (Addgene), followed by the coding sequence for eGFP and a 1.5kb 3' homology arm starting from beginning of the Rab8 coding sequence. Two guide RNAs (gRNA) were designed that cut 41bp 5' and 16bp 3' of the Rab8 ATG start site. The HDR donor plasmid and gRNAs were injected into embryos and successful CRISPR-mediated insertions were identified by fluorescence microscopy and genomic PCR (Fig. 2E-L, Supplemental Fig. 2A,B). The generated CRISPR GFP:Rab8 line is homozygous viable and fertile, indicating that CRISPR GFP:Rab8 is fully functional. Insertion of eGFP at the genomic Rab8 locus reveals that endogenous Rab8 behaviors are similar to those of the UASp-YFP:Rab8 transgene: Rab8 initially localizes to a mobile, cytoplasmic punctate population and

transitions to an association with the plasma membrane during the formation of both syncytial and cellularization furrows (Fig. 2E-L).

Disruption of Rab8 leads to a failure of furrow ingression and F-actin network formation

Both fixed and live imaging of Rab8 structures in the early embryo demonstrate dynamic behaviors and a strong association with the ingression of membrane furrows. This led us to examine the effects of Rab8 knockdown on furrow formation. We performed knockdown experiments using RNAi targeted against Rab8. dsRNA was introduced by microinjection into an otherwise WT background and embryos were scored for defective phenotypes (Fig. 3A). Three different dsRNAs directed against Rab8 were used, and all dsRNAs demonstrated a severe disruption in embryonic development (Fig. 3). Importantly, the majority of dsRNA injected embryos arrested at stages requiring furrow ingression. 40% of embryos injected with SNAPDRAGON-designed Rab8 dsRNA arrested during syncytial divisions (Fig. 3A, n=89), while 56% arrested during cellularization (Fig. 3A).

We also used the endogenous CRISPR GFP:Rab8 to address Rab8 function by co-expressing either deGradFP or GFP TRiP shRNAi in a homozygous CRISPR GFP:Rab8 background (Supplemental Fig. 3). Again, a deep disruption of development occurred in the early embryonic stages during which furrow formation is highly active, with 72% of deGradFP expressing embryos at 18˚C arresting during the syncytial divisions (Supplemental Fig. 3A). It is interesting to note that deGradFP expression produces a stronger defect than GFP TRiP; a similar result has been observed by Nagarkar-Jaiswal and colleagues (Nagarkar-Jaiswal et al., 2015).

To examine the early arrest defects more closely, dsRNA was introduced by microinjection into embryos expressing Histone:RFP and GFP:Actin-Binding-Domain of Moesin (GFP:MoeABD). This allowed the visualization of chromosomal behaviors and the ingressing furrows concurrently during development. As compared to control-injected embryos, Rab8 RNAi has a dramatic effect on the formation of furrows. In control-injected (Rhodopsin3 dsRNA) embryos, syncytial furrows form and ingress during cycles 10-13 to prevent chromosomal mixing and provide spindle anchor points during nuclear divisions (Fig. 3B). In Rab8 knockdown embryos, no

observable furrow formation occurred and fusions between adjacent nuclei were observed (Fig. 3C). The cortical F-actin that would normally associate apically with ingressing furrows is completely disrupted in these severely affected embryos (Fig. 3C). Nuclei aggregated following aberrant division cycles and subsequently dropped from their subcortical positions (Fig. 3C). Similar defects in furrow formation were observed in CRISPR GFP:Rab8 embryos expressing deGradFP or GFP TRiP shRNAi (Supplemental Fig. 3B,C). These knock-down experiments demonstrate that Rab8 has a vital role in directing the formation and ingression of furrows in the early embryo.

Rab8 populations display partial coincidence with recycling endosomes and the Golgi

Previous reports have shown the functional requirement of REs and the Golgi during furrow ingression in the early embryo (Sisson et. al., 2000; Pelissier et. al., 2003; Riggs et al., 2003; Cao et al., 2008). Given the transition that Rab8 exhibits from cytoplasmic puncta to an association with the plasma membrane, we posited that Rab8 may link internal membrane stores with delivery to the cell surface. This led us to determine whether Rab8 structures are coincident with the RE or Golgi. Immunostaining against CRISPR GFP:Rab8 and Rab11, a RE marker, show that these proteins are largely present in distinct puncta during early cellularization (Fig. 4A-F). However, a small percentage (~20%) of cytoplasmic puncta colocalize for both Rab8 and Rab11 (Fig. 4A-F, Supplemental Fig. S4). This is observable in the distance plots as the small increase in Rab8 at Rab11 maxima and vice versa (Fig. 4B,C,E,F). This coincidence increases as embryos enter fast phase, a period of rapid membrane addition (Fig. 4D, Supplemental Fig. S4; Lecuit and Wieschaus, 2000). During this period, Rab11 puncta increase in size and accumulate in an apical position above the nuclei. Rab8 often appears to colocalize in small subdomains of larger Rab11 structures (Fig. 4D). Indeed, when only larger Rab11 structures (10-26 pixels, pixel size= 0.056µm/pixel) are quantitated, the number of larger Rab11 aggregates that possess a subdomain of coincident Rab8 rises to 64% (Supplemental Fig. S4). These results suggest that there may be a transient interaction between Rab11 and Rab8 compartments, and that this interaction is more prevalent during mid to late cellularization stages when cytoplasmic membrane stores are mobilized.

Rab8 also forms a distinct compartment from the Golgi. Rab8 vesicle populations show little association with Golgi compartments during early cellularization (Fig. 4G-I, Supplemental Fig. S4). However, again during the fast phase of cellularization, the percent coincidence with the Golgi marker Lva rises from 1-2% to ~11% (Fig. 4J-L, Supplemental Fig. S4). This can be observed in the distance plots in the mild depletion of Rab8 compartments distant from Rab11 maxima, and the mild increase in Rab8 compartments near Rab11 maxima (Fig. 4K,L). Once again, the slight colocalization between Rab8 puncta and Golgi would be consistent with a possible transient interaction between Rab8 and the Golgi that occurs with higher frequency in embryos undergoing the fast phase of cellularization.

Rab8 function is required for exocytic membrane addition

The transition of Rab8 to the cell periphery during furrow ingression and the association of Rab8 with internal membrane stores such as Rab11 and the Golgi led us to ask if Rab8 is responsible for delivering the membrane that is necessary for furrow ingression. We therefore asked if Rab8 regulates membrane addition during furrow ingression. To this end, we performed Rab8 RNAi in a Gap43:mCherry background. Gap43:mCherry is a membrane marker which consists of a 20 amino acid peptide containing a double palmitoylation sequence which directs the mCherry protein to furrows and the apical plasma membrane (Martin et al., 2010; Holly et al., 2015; Fig. 5A, Movie S4). Upon knockdown of Rab8, trafficking of Gap43:mCherry to the cell surface is severely disrupted (Fig. 5B, Movie S5). Gap43:mCherry remains in cytoplasmic puncta and does not traffic to the cell surface when Rab8 function is disrupted (Fig. 5B). These results suggest that Rab8 indeed functions as a regulator of exocytic trafficking of membrane during furrow formation.

Rab8 localization to the plasma membrane is GTPase-activity dependent

To examine how the GTP state of Rab8 directs its activity, we examined the localization of GTPase or GDP-dissociation deficient mutants. We hypothesized that GTP-bound (CA) Rab8 represented the active population and would associate with those compartments in which Rab8 is directing membrane dynamics. Likewise, GDP-bound (DN) Rab8 would most likely represent inactive pools of the protein. We therefore performed live imaging and immunostaining against these activity-deficient

mutants of Rab8 in order to examine how the GTP state affects the localization of Rab8 in relation to other compartments involved in furrow ingression.

We expressed CA or DN versions of YFP-tagged Rab8 in embryos to examine changes in protein behavior over time. Immunostaining revealed that Rab8 CA (GTPase deficient) forms similar structures to Rab8 WT (compare Fig. 6A,B and 2C,D). However, it can be noted that the association with the cell periphery arises earlier, during the slow phase of cellularization, as opposed to the fast-phase in WT embryos (compare Fig. 6B and 2B). Immunostaining of Rab8 DN (GDP-dissociation deficient) revealed large aggregates that localize to the apical cytoplasm of the cell (Fig. 6C). Very low levels of Rab8 DN can also be seen at the plasma membrane when stained embryos are imaged at high gain settings (Fig. 6D).

Effects of GTPase activity on Rab8 behavior were also examined in whole mount embryos expressing either Rab8 CA or Rab8 DN over time. Again, Rab8 CA showed similar behaviors to WT. During early cellularization, Rab8 CA exists in punctate populations before transitioning to the cell periphery and where it persists until the end of cellularization (Fig. 6E-E’’’). Expression of Rab8 DN in whole embryos shows the progressive appearance of apical cytoplasmic aggregates, which grow and persist throughout the cellularization process (Fig. 6F-F’’’). The above results suggest that active, GTP-bound Rab8 localizes to puncta and associates with the plasma membrane while inactive, GDP-bound Rab8 is cytoplasmic.

We also examined how GTPase activity affects the localization of Rab8 in relation to the RE and Golgi. Rab8 CA forms distinct compartments from both the RE and Golgi (Fig. 6G,J). Rab8 DN also does not appear to associate with RE or Golgi compartments (Fig. 6H,I,K,L). However, Rab11 compartments are enlarged in embryos expressing Rab8 DN when compared to those in Rab8 CA and WT (Fig. 6H,I). This enlargement is apparent both in apical planes (Fig. 6H) and more basal sections (Fig. 6I). These results would be consistent with a requirement for Rab8 in the trafficking of membrane from the RE to the ingressing furrow, and further supports a possible interaction between the two compartments.

Sec5 and Rab11 function are required for targeting of Rab8 to the cell cortex

As the exocyst complex is required for targeted membrane addition during furrow formation in the early embryo (Murthy et al., 2010; Holly et al., 2015) and Rab8 can bind to the Sec15 subunit of the exocyst during lumen formation and ciliogenesis (Bryant et al., 2010; Knödler et al., 2010; Feng at al., 2012), we asked if exocyst complex function is required for Rab8 dynamics in the early embryo. RNAi against Sec5 was performed in a YFP:Rab8 background and imaged over time. These experiments resulted in a failure of Rab8 to transition from cytoplasmic puncta to a peripheral association (Fig. 7B-B’’’), as compared to injection controls (Fig. 7A-A’’’), suggesting that Rab8 may utilize the exocyst to properly localize to the plasma membrane.

The RE has been previously implicated in being required for membrane addition during cellularization (Pelissier et al., 2003). We thus performed RNAi against Rab11 to ask if disruption of the RE resulted in changes in Rab8 protein behavior. Similar to Sec5 knock-down, disruption of Rab11 led to a loss of Rab8 transitioning into an association with the plasma membrane (Fig. 7C-C’’’), consistent with Rab8 requiring Rab11 source membrane or a Rab11-recruited GEF activity. Interestingly, when RNAi of Rab8 is performed in a YFP:Rab11 background, compared to controls (Fig. 7D), Rab11 puncta are present (Fig. 7E), but appear to grow slightly enlarged over time (Fig. 7E”, E’’’, yellow arrowhead). Taken together, these data suggest that Rab8 requires both exocyst complex and RE function in order to traffic to the cell surface. It is possible that Rab8 requires the exocyst as a targeting and tethering cue in order to properly associate with the plasma membrane, while utilizing Rab11 as a source of membrane that permits Rab8 activity and trafficking to the cell cortex. The slight enlargement of RE puncta in Rab8 DN and Rab8 RNAi backgrounds also strengthens the possibility that Rab8 functions to mediate the delivery of membrane from RE stores to the plasma membrane during furrow ingression.

Discussion

Here we identify Rab8 as a critical component of a trafficking pathway that directs furrow ingression in the early embryo of *Drosophila*. Rab8 demonstrates striking dynamic behaviors in the early embryo, existing in small punctate structures that then transition to an association with the plasma membrane. This transition correlates with the ingression of syncytial furrows as well as the onset of the fast phase during cellularization, suggesting that a common membrane trafficking mechanism is required during each of these processes. We have also previously observed that syncytial furrows ingress at a similar rate as that reported for fast phase (Holly et al., 2015). Peripheral Rab8 is specifically found in an apicolateral region on cellularizing furrows, the region of the furrow to which membrane addition is known to occur (Lecuit and Wieschaus, 2000; Sisson et al., 2000; Pelissier et al., 2003), and furrow formation fails when Rab8 function is disrupted. Additionally, when Rab8 function is disrupted, exocytic delivery to the cell surface fails and cargo proteins remain in cytoplasmic puncta. These results suggest a model in which Rab8 directs targeted membrane addition to furrows that permits furrow ingression (Fig. 8).

Previous studies have shown that membrane addition is required during cellularization and is provided through RE and Golgi trafficking pathways (Sisson et al., 2000; Pelissier et al., 2003, Riggs et al., 2003). However, a confounding aspect of these known membrane pathways is that they do not display an association with, or movement to, ingressing furrows. Immunostaining against either the RE or Golgi and Rab8 indicated that Rab8 largely exists in distinct compartments. However, quantification of colocalization revealed that Rab8 displays a small, but reproducible, coincidence with the RE and Golgi (10-20% of compartments quantified during fast phase), and Rab8 appeared to mark subdomains of larger Rab11 compartments. It is therefore possible that these populations have transient interactions with each other. Indeed, Rab trafficking pathways often function through compartments changing their identity by dissociating with one Rab and acquiring another (Rink et. al., 2005), and Rab11 has been demonstrated to bind and stimulate a Rab8 GEF, Rabin8, during ciliogenesis (Knodler et al., 2010). We also observed that disrupting the function of Rab11 resulted in the failure of Rab8 to transition from the cytoplasmic puncta to the plasma membrane, and that Rab8 puncta appeared to be stationary and inactive. Conversely, when Rab8 function was disrupted, either in Rab8 DN embryos or by

Rab8 RNAi injection, a mild enlargement of the Rab11 recycling endosome was observed. These results would be consistent with Rab8 serving to connect membrane cytoplasmic stores to the ingressing furrow (Fig. 8B).

Rab8 directed membrane trafficking to the plasma membrane may occur through its binding and tethering of vesicles to the exocyst complex (Fig. 8C). During lumen formation and ciliogenesis in mammalian cells, Rab8 binds to the Sec15 subunit of the exocyst complex (Bryant et al., 2010; Knodler et al., 2010; Feng at al., 2012). This function and interaction may be preserved during cellularization as the Sec5 subunit of the exocyst complex is required for cellularization, and Sec5 localizes to the apicolateral region of the cellularizing furrow in the area where membrane addition and Rab8 localization occurs (Murthy et al., 2010). Indeed, disruption of Sec5 by RNAi leads to a failure of Rab8 to transition into a cortical association. RalA GTPase function, a critical factor in directing exocyst complex assembly, is also required for Rab8 localization to the cell cortex (Moskalenko et al., 2002, Moskalenko et al., 2003; Fukai et al., 2003; Holly et al., 2015). Additionally, disruption of the Exo84 exocyst subunit in the fly embryo leads to an enlargement of Rab11 REs, which resembles the defects observed in Rab8 DN expressing embryos (Blankenship et al., 2007). In summary, Rab8 may direct vesicular traffic from the RE/Golgi to exocyst tethering complexes on the ingressing furrow (Fig. 8).

Syncytial furrow formation and the cellularization network are essentially specialized forms of cytokinetic furrows (Schejter and Wieschaus, 1993; Sullivan and Theurkauf, 1995). It is therefore interesting to contrast our findings to those in classical cytokinetic furrows. It is clear that ingressing furrows in both cytokinetic cells as well as in the early fly embryos require membrane trafficking pathways as part of the furrowing mechanism (Lecuit and Wieschaus, 2000); Albertson et al., 2005; Prekeris and Gould, 2008). However, syncytial furrow formation is reported to be independent of Myosin II function, while cytokinetic furrows and cellularization require the activation of Myosin II motor proteins (Warn et al., 1990; Keihart, 1990; Young et al., 1991; Royou et al., 2004). Rab8 localizes to, and is required for, both syncytial furrows and the cellularization network. It is therefore possible to suggest that rapid membrane addition through a Rab8-dependent mechanism may provide an important portion of the additional surface area that the deeply ingressing furrows in the early

embryo require. It may further be that targeted membrane addition provides some of the force for the ingression of syncytial furrows that lack Myosin II function, although it is also clear that membrane ingression in the early embryo additionally requires the function of the F-actin cytoskeleton (Sokac and Wieschaus, 2008a; Sokac and Wieschaus, 2008b; Yan et al., 2013; Reversi et al., 2014). A requirement for Rab8 function at cytokinetic furrows has been less clear, although it has been shown that Rab8 vesicles are transported along microtubules to the midbody (Pohl and Jentsch, 2008), and siRNAs directed against Rab8 that produce binucleate cells were identified in a systematic RNAi screen for proteins that are required for mitosis in human cells (Neuman et al., 2010). It is interesting to note that several Rab proteins (Rab13, Rab15, Rab36) that possess high similarity in either identity or function to Rab8 exist in the human genome but do not appear to be present in *Drosophila* (Chan et al., 2011). A focus for further studies will be teasing apart the contributions of Rab8-dependent membrane trafficking and F-actin and Myosin II function in directing cleavage furrow ingression.

Materials and Methods

Fly Stocks and Genetics

Flies were maintained at 25°C by standard procedures. UAS transgenic flies were crossed to matαTub-Gal4VP16 67C;15 (D. St. Johnson) maternal driver females or Rab8>Gal4 (Fig. 1, Bloomington) and second generation embryos were analyzed. UAS-deGradFP; CRISPR:GFP:Rab8 or UAS-GFP TRiP; CRISPR:GFP:Rab8 were crossed to matαTub-Gal4VP16 67C; CRISPR:GFP:Rab8 and second generation embryos were analyzed.

Fly Stocks: UASp-YFP:Rab8, UASp-YFP:Rab8 T22N, UASp-YFP:Rab8 Q67L, UASp-YFP:Rab11, sqh-Histone:RFP, UASp-deGradFP 58740, UAS-GFP TRiP Valium 20 41555 (Bloomington); sqh-GFP:MoesinABD (Kiehart et al., 2000); sqh-mCh:MoesinABD (Millard and Martin, 2008). Gap43:mCherry (Martin et al., 2010).

Construction of CRISPR GFP:Rab8 transgenic line

To create transgenic lines of CRISPR GFP:Rab8, a genomic DNA HDR donor plasmid was generated comprising the genomic DNA 1.5 kb upstream of the Rab8 ATG start site cloned into pBluescript KS, followed by the coding sequence of GFP and the 1.5kb 3' of the Rab8 ATG start site. In total, 3kb of the genomic Rab8 locus was cloned and inserted into the pCasper4 plasmid, along with the 717 bp CDS of eGFP, using standard PCR and cloning protocols to create the HDR donor plasmid. Two GuideRNA sequences that serve to guide the Cas9 nuclease enzyme to specific genome locations were designed as according to Gokcezade et al. (2014) and inserted into pU6-BbsI-gRNA. All constructs were sequence-verified (UC Denver Core Sequencing).

Guide RNAs for CRISPR GFP:Rab8

5'chiRNA-1	CTTCGAACAGATAGTCGTAGGTTT
3'chiRNA-1	AAACAAACCTACGACTATCTGTTC
5'chiRNA-2	CTTCGCCCGATAATAGTGCTTAGC
3'chiRNA-2	AAACGCTAACGACTATTATCGGGC

Guide RNAs (100ng/µl) and GFP:Rab8 plasmid (150ng/µl) were co-injected into Cas9-expressing flies (y, nos-Cas9, w; BDSC #54591) by BestGene. Surviving adults were crossed to Sp/Cyo; Dr/Tm3 flies in a series of crosses to create possible insertion lines. Embryos from these individual lines were tested for fluorescence using a

spinning-disk confocal microscope, and insertion into the genome was verified by PCR (see below). Successful insertions were relatively rare: 270 lines were scored before recovery of CRISPR GFP:Rab8.

Cloning primers for HDR donor GFP:Rab8

5'CRISPRRab8(1)SpeI	GGACTAGTAAAATGCTCCCCTTTCATTAT
3'CRISPRRab8(1)BamHI	CGGGATCCTTTGTGTGCTTTTGCGGTAG
5'CRISPRGFPBamHI	CGGGATCCGTTGTACAGCTCGTCCATGC
3'CRISPRGFPSalI	ACGCGTCGACCGCCCCGCCCTGCCACTCAT
5'CRISPRRab8(2)SalI	ACGCGTCGACATGGCCAAAACCTACGACTA
3'CRISPRRab8(2)KpnI	GGGGTACCTATATAAATAAAATGTTTGT

PCR-verification of CRISPR GFP:Rab8 transgenic line

PCR primers to verify correct insertion of GFP into the *Drosophila* genome via CRISPR were designed in the following manner. The 5' primer was targeted against a genomic region outside of that which was cloned into the HDR donor GFP:Rab8 plasmid (1.7kb upstream of Rab8 start codon), while the 3' primer was targeted against a region within the GFP coding sequence. Thus, successful PCR product could only be produced when eGFP has been integrated into the genomic Rab8 locus. Three primer pairs were designed in this manner (NIH, Primer Design Tool) and PCR was performed in both CRISPR GFP:Rab8 flies and control OreR flies.

Primers for PCR Verification of CRISPR GFP:Rab8 insertion

5'PCR-1	*TGACATGCAGAATTAAAAGCCC*
3'PCR-1	*CGGACACGCTGAACTTGTG*
5'PCR-2	*ATGACATGCAGAATTAAAAGCCCA*
3'PCR-2	*GTCAGCTTGCCGTAGGTGG*
5'PCR-3	*TGACATGCAGAATTAAAAGCCCAAT*
3'PCR-3	*GCTGAACTTGTGGCCGTTTAC*

Confocal microscopy and time-lapse imaging

Confocal images were acquired on an Olympus Fluoview FV1000 confocal laser scanning microscope with 40x/1.35 NA or 60x/1.42 NA objectives for fixed specimens. Time lapse imaging was performed on a spinning disk confocal from Zeiss and Solamere Technologies Group with 40x/1.3 NA or 63x/1.4 NA objectives. Embryos were imaged after dechorionation and placement on a gas permeable membrane in Halocarbon 27 oil. Live imaging was performed using exposure settings of 150-500 msec and images were acquired at either fast (< 1/sec) or slow (1/30sec) rates (see Figures and Supplemental Movie captions).

Embryo fixation and immunostaining

Embryos were dechorionated in 50% bleach solution and fixed for 1 hr 15 min at the interface of heptane and 3.7% formaldehyde in 0.1M sodium phosphate buffer (pH 7.4) before being manually devitellinized and stained with Alexa-546 phalloidin (1:200, Molecular Probes) rabbit anti-GFP (1:1000, Invitrogen), mouse anti-GFP (1:100, Molecular Probes), rabbit anti-lava (1:250, Sisson et al., 2000), rabbit anti-Rab11 (1:1000, Satoh et al., 2005), Hoescht (1:500, Sigma), mouse anti-Nrt (1:1, DSHB) or mouse anti-Sec5 (1:35; Murthy et al., 2010). Conjugated secondary antibodies Alexa-488, Alexa-546 or Alexa-568 were used at 1:500 (Molecular Probes). Embryos were mounted in Prolong Gold with DAPI (Molecular Probes).

Fixed and time lapse embryo analysis and quantification of vesicle colocalization

Confocal and spinning disk images were edited using Adobe Photoshop. Channels for fixed images were uniformly leveled for optimal channel appearance. Time-lapse images were leveled with Photoshop to show optimal protein populations, or were processed with identical settings to permit comparisons in protein levels.

Automated quantitation was performed as follows. In each color channel, local intensity maxima were detected using a wavelet-based detection method as used in (Loerke et al., 2009), which is based on *a trou* detection first proposed by (Olivo-Marin, 2002). For each channel, a Euclidian distance map was then calculated with respect to the detected maxima. Using this distance map in combination with the raw intensity images, we interpolated the average intensity-vs-distance function (using Gaussian smoothing with σ=0.5 pixels) from all pixels in the image. This interpolation was performed for the intensity and the distance map from the same channel (e.g. red intensity vs distance from red maxima), but also for the combination of intensity and the distance map from the other channel (e.g. red intensity vs distance from green maxima). In addition, we calculated a distance map for randomly placed maxima positions (which was performed in practice by switching the x and y-coordinates of the true maxima) that removes all spatial correlation of the intensity signal. The error bars shown in the figure represent the standard deviation of cell-to-cell variation of the intensity function for a given condition.

The associated p-value is the p-value of a 2-sided T-test between the other-channel intensity function and the random-position intensity function (both at distance zero),

i.e. the p-value tells us whether the measured colocalization of the other-channel intensity function is significantly different from a spatially random (i.e. uncolocalized) intensity distribution. A minimum of 10 individual images collected from at least 5 different embryos was analyzed for each stage and immunostain.

Distance maps can give a probabilistic determination of coincidence, but cannot distinguish objects and give a segmented analysis of percent colocalization other than by a pixel-by-pixel basis. We therefore additionally used manual identification of individual Rab8, Rab11, and Lva puncta. Manual quantification of individual objects and coincidence between Rab8 vesicle populations and Rab11 RE and Golgi populations was performed using Adobe Photoshop. Quantification was performed by selecting puncta between 2 and 26 pixels (pixel size = 0.056µm/pixel) in size in set areas of 5x5 grids. The selected puncta were then overlaid with the opposing channel and colocalizing puncta counted. Average colocalization was found by performing a weighted average calculation from a minimum of 6 individual images collected from 3 different embryos and standard deviations were plotted.

Manual vesicle counts of YFP:Rab8 during syncytial divisions or cellularization stages were performed in the same manner as colocalization counts described above. Still frames from the onset of a syncytial stage/slow-phase, prior to cortical transition, first appearance of cortical array and persistence of cortical array were chosen and all vesicles were counted from a 512x512 pixel image.

siRNA Preparation

Primers for siRNA treatments were chosen to represent independent regions of Rab8 (5'UTR) or through the use of the SNAPDRAGON RNAi design program that bioinformatically selects against off-target affects (DSRC, Harvard). siRNA primers for Rh3, Rab11 and Sec5 were designed also using the SNAPDRAGON system. dsRNA was made using a Megascript T7 transcription kit (Ambion) and purified using Qiagen RNAeasy columns. A final concentration was determined with a NanoDrop ND1000 Spectrophotometer.

RNAi Treatments

Embryos were prepared in the same manner as for live imaging and then glued to a coverslip using heptane glue. Embryos were dehydrated for ~12 minutes, and then injected with siRNA against Rh3 (13 µM), Rab8 (550bp, 13µM; 5'UTR, 11µM; SNAP, 13µM), Rab11 (13µM) or Sec5 (18µM).

Embryo scoring and analysis

Embryos were collected on apple juice agar plates, and development was followed and scored under Halocarbon 27 oil on a Zeiss dissecting microscope with transillumination. Pooled data from multiple trials were summed, and RNAi scoring data (Fig. 3) was tested for statistical significance using a two-dimensional contingency table with a X^2 test with α=0.05. Tests were performed in two ways: 1. All data was tested to determine if changes in phenotypic proportions seen were significant, which resulted in $p < 0.0001$. 2. Both RNAi treatment groups were tested against Rhodopsin control treatment to determine if changes in phenotypic proportions were significant in relation to control proportions. All tests gave $p < 0.0001$.

Acknowledgements

We are grateful to the generous colleagues who supplied us with antibodies and fly lines: Hugo Bellen (Houston, TX, USA), Don Ready (West Lafayette, IN, USA), John Sisson (Austin, TX, USA), Adam Martin (Cambridge, MA, USA), Daniel Kiehart (Durham, NC, USA), Tom Millard (Manchester, Greater Manchester, UK) and Tom Schwarz (Cambridge, MA). We gratefully acknowledge the work of Cayla Jewett in pioneering CRISPR and deGradFP techniques in the lab. Thanks are due to Dinah Loerke (Denver, CO, USA), Alan Zhu (Cleveland, OH, USA), and the Blankenship lab for suggestions and critical reading of the manuscript. This work was supported by an NIH R01 GM090065 to J.T.B.

Author Contribution

J.T.B. is responsible for designing the concept and approaches used in the above paper. L.M.M. performed the experiments and data analysis with the exceptions of those that follow: H.M. and Z.Z. were responsible for performing CRISPR GFP:Rab8, Rab11, and Lva immunostains and R.M.H. and Y.X. performed CRISPR GFP:Rab8 stains and live imaging. Writing and editing of the manuscript was shared between L.M.M and J.T.B.

References

Baena-Lopez, L.A., Alexandre, C., Mitchell, A., Pasakarnis, L., and Vincent, J.P. (2013). Accelerated homologous recombination and subsequent genome modification in Drosophila. *Development*. **140**, 4818-25.

Baskys, A., Bayazitov, I., Zhu, E., Fang, L. and Wang, R. (2007). Rab-mediated endocytosis: linking neurodegeneration, neuroprotection, and synaptic plasticity? *Ann. N. Y. Acad. Sci*. **1122,** 313-329.

Bassett, A.R., Tibbit, C., Ponting, C.P., and Liu, J.L. (2013). Highly efficient targeted mutagenesis of Drosophila with the CRISPR/Cas9 system. *Cell Rep* **4**, 220-228.

Beronja, S., Laprise, P., Papoulas, O., Pellikka, M., Sisson, J., Tepass, U. (2005). Essential function of Drosophila Sec6 in apical exocytosis of epithelial photoreceptor cells. *J. Cell. Biol.* **169,** 635-646.

Blankenship, J. T., Fuller, M. T. and Zallen, J. A. (2007). The Drosophila homolog of the Exo84 exocyst subunit promotes apical epithelial identity. *J. Cell. Sci*. **120**, 3099-3110.

Bryant, D. M., Datta, A., Rodriguez-Fraticelli, A. E., Peränen, J., Martín-Belmonte, F. and Mostov, K. E. (2010). A molecular network for de novo generation of the apical surface and lumen. *Nat. Cell. Biol.* **12**, 1035-1045.

Cao, J., Albertson, R., Riggs, B., Field, C. M. and Sullivan, W. (2008). Nuf, a Rab11 effector, maintains cytokinetic furrow integrity by promoting local actin polymerization. *J. Cell. Biol*. **182**, 301-313.

Chan, C-C., Scoggin, S., Wang, D., Cherry, S., Dembo, T., Greenberg, B., Jin, E.J., Kuey, C., Lopex, A., Mehta, S.Q., et al. (2011). Systematic Discovery of Rab GTPases with Synaptic Functions in Drosophila. *Curr. Biol.* **21,** 1704-1715.

Chen, S., Liang, M.C., Chia, J.N., Ngsee, J.K., and Ting, A.E. (2001). Rab8b and Its Iteracting Partner TRIP8b Are Involved in Regulated Secretion in AtT20 Cells. *J. Biol. Chem.* **276,** 13209-13216.

Fabrowski, P., Necakov, A.S., Mumbauer, S., Loeser, E., Reversi, A., Streichan, S., Briggs, J.A., and De Renzis, S. (2013). Tubular endocytosis drives remodelling of the apical surface during epithelial morphogenesis in *Drosophila*. *Nat Commun.* **4**, 2244.

Feng, S., Knödler, A., Ren, J., Zhang, J., Zhang, X., Hong, Y., Huang, S., Peränen, J. and Guo, W. (2012). A Rab8 guanine nucleotide exchange factor-effector interaction network regulates primary ciliogenesis. *J. Biol. Chem.* **287**, 15602-15609.

Figard, L., Xu, H., Garcia, H. G., Golding, I., Sokac, A. M. (2013). The plasma membrane flattens out to fuel cell-surface growth during *Drosophila* cellularization. *Dev Cell*. **27**, 648-655.

Foe, V. E., Field, C. M. and Odell, G. M. (2000). Microtubules and mitotic cycle phase modulate spatiotemporal distributions of F-actin and myosin II in Drosophila syncytial blastoderm embryos. *Development.* **127**, 1767-1787.

Fukai, S., Matern, H. T., Jagath, J. R., Scheller, R. H. and Brunger, A. T. (2003). Structural basis of the interaction between RalA and Sec5, a subunit of the sec6/8 complex. *EMBO J.* **22**, 3267-3278.

Gokcezade, J., Grzegorz, S., Duchek, P. (2014). Efficient CRISPR/Cas9 Plasmids for Rapid and Versatile Genome Editing in Drosophila. *G3.* **4,** 2279-2282.

Gratz, S.J., Cummings, A.M., Nguyen, J.N., Hamm, D.C., Donohue, L.K., Harrison, M.M., Wildonger, J., and O'Connor-Giles, K.M. (2013a). Genome engineering of Drosophila with the CRISPR RNA-guided Cas9 nuclease. *Genetics.* **194**, 1029-1035.

Grosshans, B. L., Andreeva, A., Gangar, A., Niessen, S., Yates, J. R. 3rd, Brennwald, P. and Novick, P.(2006). The yeast Igl family member Sro7p is an effector of the secretory Rab GTPase Sec4p. *J. Cell. Biol.* **172,** 55-66.

Hardiman, C. A., McDonough, J. A., Newton, H. J. and Roy, C. R. (2012). The role of Rab GTPases in the transport of vacuoles containing Legionella pneumophila and Coxiella burnetti. *Biochem. Soc. Trans.* **40**, 1353-1359.

Hartenstein, V. (1993). Atlas of *Drosophila* development. (New York: Cold Spring Harbor Laboratory Press).

Hattula, K., Furuhjelm, J., Tikkanen, J., Tanhuanpää, K., Laakkonen, P. and Peränen, J. (2006). Characterization of the Rab8-specific membrane traffic route linked to protrusion formation. *J. Cell. Sci*. **119**, 4866-4877.

Holly, R.M., Mavor, L.M., Zuo, Z. and Blankenship, J.T. (2015). A rapid, membrane-dependent pathway directs furrow formation through RalA in the early Drosophila embryo. *Development.* **142**, 2316-28.

Horgan, C. P. and McCaffrey, M. W. (2012). Endosomal trafficking in animal cytokinesis. *Front. Biocsci.* **1**, 1202-1206.

Huber, L.A., Dupree, P., Dotti, C.G., (1995). A Deficiency of the Small GTPase rab8 Inhibits Membrane Traffic in Developing Neurons. *Mol. Cell Biol.* **15,** 918-924.

Jafar-Nejad, H., Andrews, H.K., Acar, M., Bayat, V., Wirtz-Peitz, F., Mehta, S.Q., Knoblich, J.A., Bellen, H.J. (2005). Sec15, a component of the exocyst, promotes notch signaling during the asymmetric division of Drosophila sensory organ precursors. *Dev. Cell*. **9,** 351-363.

Kaplan, A. and Reiner, O. (2011). Linking cytoplasmic dynein and transport of Rab8 vesicles to the midbody during cytokinesis by the doublecortin domain-containing 5 protein. *J. Cell. Sci.* **124,** 1-12.

Kiehart, D.P., Ketchum, A., Young, P., Lutz, D., Alfentino, M.R., Chang, X.J, Awobuluyi, M., Pesacreta, T.C., Inoué, S, Stewart, C.T., et al. (1990). Contractile proteins in Drosophila development. *Ann. NY Acad. Sci.* **582**, 233-51

Knödler, A., Feng, S., Zhang, J., Zhang, X., Das, A., Peränen, J. and Guo, W. (2010). Coordination of Rab8 and Rab11 in primary ciliogenesis. *Proc. Natl. Acad. Sci.* USA. **107**, 6346-1651.

Langevin, J., Morgan, M.J., Sibarita, J.G., Aresta, S., Murthy, M., Schwarz, T., Camonis, J., Bellaïche, Y. (2005). Drosophila exocyst components Sec5, Sec6, and Sec15 regulate DE-Cadherin trafficking from recycling endosomes to the plasma membrane. *Dev. Cell*. **9,** 365-376.

Lecuit, T. (2004). Junctions and vesicular trafficking during Drosophila cellularization. *J. Cell. Sci.* **117**, 3427-33.

Lecuit, T. and Wieschaus, E. (2000). Polarized insertion of new membrane from a cytoplasmic reservoir during cleavage of the Drosophila embryo. *J. Cell. Biol.* **150,** 849-860.

Loerke, D., Mettlen, M., Yarar, D., Jaqaman, K., Jaqaman, H., Danuser, G., and Schmid, S.L. (2009). Cargo and dynamin regulate clathrin-coated pit maturation. *PLoS Biol.* **17**, e57.

Martin, A. C., Gelbart, M., Fernandez-Gonzalez, R., Kaschube, M., Wieschaus, E. F. (2010). Integration of contractile forces during tissue invagination. *J Cell Biol*. **188**, 735-749.

Mazumdar, A. and Mazumdar, M. (2002). How one becomes many: blastoderm cellularization in Drosophila melanogaster. *Bioessays.* **24**, 1012-22.

Millard, T. H. and Martin, P. (2008). Dynamic analysis of filopodial interaction during the zippering phase of Drosophila dorsal closure. *Development.* **135**, 621-626.

Mitra, S., Cheng, K. W., and Mills, G. B. (2011). Rab GTPases implicated in inherited and acquired disorders. *Semin. Cell Dev. Biol.* **22**, 57-68.

Moritz, O.L., Tam, B.M., Hurd, L., Peränen, J., Deretic, D., Papermaster, D.S. (2001). Mutant rab8 Impairs Docking and Fusion of Rhodopsin-bearing Post-Glogi Membranes and Causes Cell Death of Transgeneic *Xenopus* Rods. *Mol. Biol. Cell.* **12,** 2341-2351.

Moskalenko, S., Henry, D. O., Rosse, C., Mirey, G., Camonis, J. H. and White, M. A. (2002). The exocyst is a Ral effector complex. *Nat. Cell Biol.* **4**, 66-72.

Moskalenko, S., Tong, C., Rosse, C., Mirey, G., Formstecher, E., Daviet, L., Camonis, J. and White, M. A. (2003). Ral GTPases regulate exocyst assembly through dual subunit interactions. *J. Biol. Chem.* **278**, 51743-51748.

Murthy, M., Teodoro, R.O., Miller, T.P. and Schwarz, T.L. (2010). Sec5, a member of the exocyst complex, mediates Drosophila embryo cellularization. *Development*. **137**, 2773-2783.

Nachury, M.V., Loktev, A.V., Zhang, Q., Westlake, C.J., Peränen, J., Merdes, A., Slusarski, D.C., Scheller, R.H., Bazan, J.F., Sheffiled, V.C., Jackson, P.K. (2007). A Core Complex of BBS Proteins Cooperates with the GTPase Rab8 to Promote Ciliary Membrane Biogenesis. *Cell.* **129,** 1201-1213.

Nagarkar-Jaiswal, S., Lee, P.T., Campbell, M.E., Chen, K., Anguiano-Zarate, S., Gutierrez, M.C., Busby, T., Lin, W.W., He, Y., Schulze, K.L., Booth, B.W., Evans-Holm, M., Venken, K.J., Levis, R.W., Spradling, A.C., Hoskins, R.A., Bellen, H.J. (2015). A library of MiMICs allows tagging of genes and reversible, spatial and temporal knockdown of proteins in Drosophila.
Elife. **31**, 4.

Neumann B, Walter T, Hériché JK, Bulkescher J, Erfle H, Conrad C, Rogers P, Poser I, Held M, Liebel U, Cetin C, Sieckmann F, Pau G, Kabbe R, Wünsche A, Satagopam V, Schmitz MH, Chapuis C, Gerlich DW, Schneider R, Eils R, Huber W,Peters JM, Hyman AA, Durbin R, Pepperkok R, Ellenberg J. (2010). Phenotypic profiling of the human genome by time-lapse microscopy reveals cell division genes. *Nature.* **46**, 721-7.

Olivo-Marin, J.C. (2002). Extraction of spots in biological images using multiscale products. *Pattern Recognition*. **35**, 1989-1996.

Pelissier, A., Chauvin, J. P. and Lecuit, T. (2003). Trafficking through Rab11 endosomes is required for cellularization during Drosophila embryogenesis. *Curr. Biol*. **13**, 1848-1857.

Peranen, J. (2011). Rab8 GTPases as a regulator of cell shape. *Cytoskeleton*. **68**, 527-539.

Peranen, J., Auvinen, P., Virta, H., Wepf, R. and Simons, K. (1996). Rab8 promotes polarized membrane transport through reorganization of actin and microtubules in fibroblasts. *J. Cell. Biol.* **135,** 153-167.

Pfeffer, S. (2005). A model for Rab GTPase localization. *Biochem. Soc. Trans.* **33**, 637-630.

Pohl, C. and Jentsch, S. (2008). Final stages of cytokinesis and midbody ring formation are controlled by BRUCE. *Cell.* **132,** 832-845.

Recchi, C. and Seabra, M.C. (2012). Novel functions for Rab GTPases in multiple aspects of tumour progression. *Biochem. Soc. Trans.* **40,** 1398-1403.

Reversi, A., Loeser, E., Subramanian, D., Schultz, C., De Renzis, S. (2014). Plasma membrane phosphoinositide balance regulates cell shape during Drosophila embryo morphogenesis. *J Cell Biol.* **205,** 395-408.

Riggs, B., Rothwell, W., Mische, S., Hickson, G. R., Matheson, J., Hays, T. S., Gould, G. W. and Sullivan, W. (2003). Actin cytoskeleton remodeling during early Drosophila furrow formation requires recycling endosomal components Nuclear-fallout and Rab11. *J. Cell. Biol*. **163**, 143-154.

Rink, J., Ghigo, E., Kalaidzidis, Y. and Zerial, M. (2005). Rab conversion as a mechanism of progression from early to late endosomes. *Cell*. **122**, 735-749.

Royou, A., Field, C., Sisson, J. C., Sullivan, W. and Karess, R. (2004). Reassessing the role and dynamics of nonmuscle myosin II during furrow formation in early Drosophila embryos. *Mol. Biol. Cell.* **15**, 838-850.

Satoh, A. K., O'Tousa, J. E., Ozaki, K. and Ready D. F. (2007). Rab11 mediates post-Golgi trafficking of rhodopsin to the photosensitive apical membrane of Drosophila photoreceptors. *Development.* **132,** 1487-1497.

Schejter, E. D. and Wieschaus, E. (1993). Functional elements of the cytoskeleton in the early Drosophila embryo. *Annu. Rev. Cell. Biol*. **9**, 67-99.

Sisson, J. C., Field, C., Ventura, R., Royou, A. and Sullivan, W. (2000). Lava lamp, a novel peripheral golgi protein, is required for Drosophila melanogaster cellularization. *J. Cell. Biol*. **151**, 905-918.

Sokac, A.M and Wieschaus, E. (2008a). Local actin-dependent endocytosis is zygotically controlled to initiate Drosophila cellularization. *Dev. Cell.* **14,** 775-786.

Sokac, A. M. and Wieschaus, E. (2008b). Zygotically controlled F-actin establishes cortical compartments to stabilize furrows during *Drosophila* cellularization. *J. Cell. Sci.* **121**, 1815-1824.

Sullivan, W., Theurkauf, W. E. (1995). The cytoskeleton and morphogenesis of the early Drosophila embryo. *Curr Opin Cell Biol*. **7**, 18-22.

Warn, R.M., Warn, A., Planques, V., Robert-Nicoud, M . (1990). Cytokinesis in the early Drosophila embryo. *Ann. NY Acad. Sci.* **582**, 222-32.

Wu, S., Mehta, S.Q., Pichaud, F., Bellen, H.J., Quiocho, F.A. (2005). Sec15 interacts with Rab11 via a novel domain and affects Rab11 localization in vivo. *Nat. Struct. Mol. Biol.* **12,** 879-885.

Yan, S., Lv, Z., Winterhoff, M., Wenzi, C., Zobel, T., Faix, J., Bogdan, S., Grosshans, J. (2013). The F-BAR protein Cip4/Toca-1 antagonizes the formin Diaphanous in membrane stabilization and compartmentalization. *J. Cell Sci.* **126,** 1796-1805.

Yeaman, C., Grindstaff, K.K., Wright, J.R., Nelson, W.J. (2001). Sec 6/8 comoplexes on trans-Golgi network and plasma membrane regulate late stages of exocytosis in mammalian cells. *J. Cell Biol.* **155,** 593-604.

Yeaman C., Grindstaff, K.K., Nelson, W.J. (2004). Mechanism of recruiting Sec6/8 (exocyst) complex to the apical junctional complex during polarization of epithelial cells. *J. Cell Sci.* **117,** 559-570.

Yoshimura, S-i., Egerer, J., Fuchs, E., Haas, A.K., Barr, F.A. (2007). Functional dissection of Rab GTPases involved in primary cilium formation. *J. Cell Biol.* **178,** 363-369.

Zhang, X.M., Ellis, S., Sriratana, A., Mitchell, C.A., Rowe, T. (2004). Sec15 is an effector for the Rab11 GTPase in mammalian cells. *J Biol Chem.* **279,** 4302-43034.

Zhang, J., Schulze, K. L., Hiesinger, P. R., Suyama, K., Wang, S., Fish, M., Acar, M., Hoskins, R. A., Bellen, H. J. and Scott, M. P. (2007). Thirty-one flavors of Drosophila rab proteins. *Genetics.* ***176***, 1307-13022.

Zhang, J., Fonovic, M., Suyama, K., Bogyo, M., Scott, M.P. (2009). Rab35 controls actin bundling by recruiting fascin as an effector protein. *Science.* **325,** 1250-1254

Figures

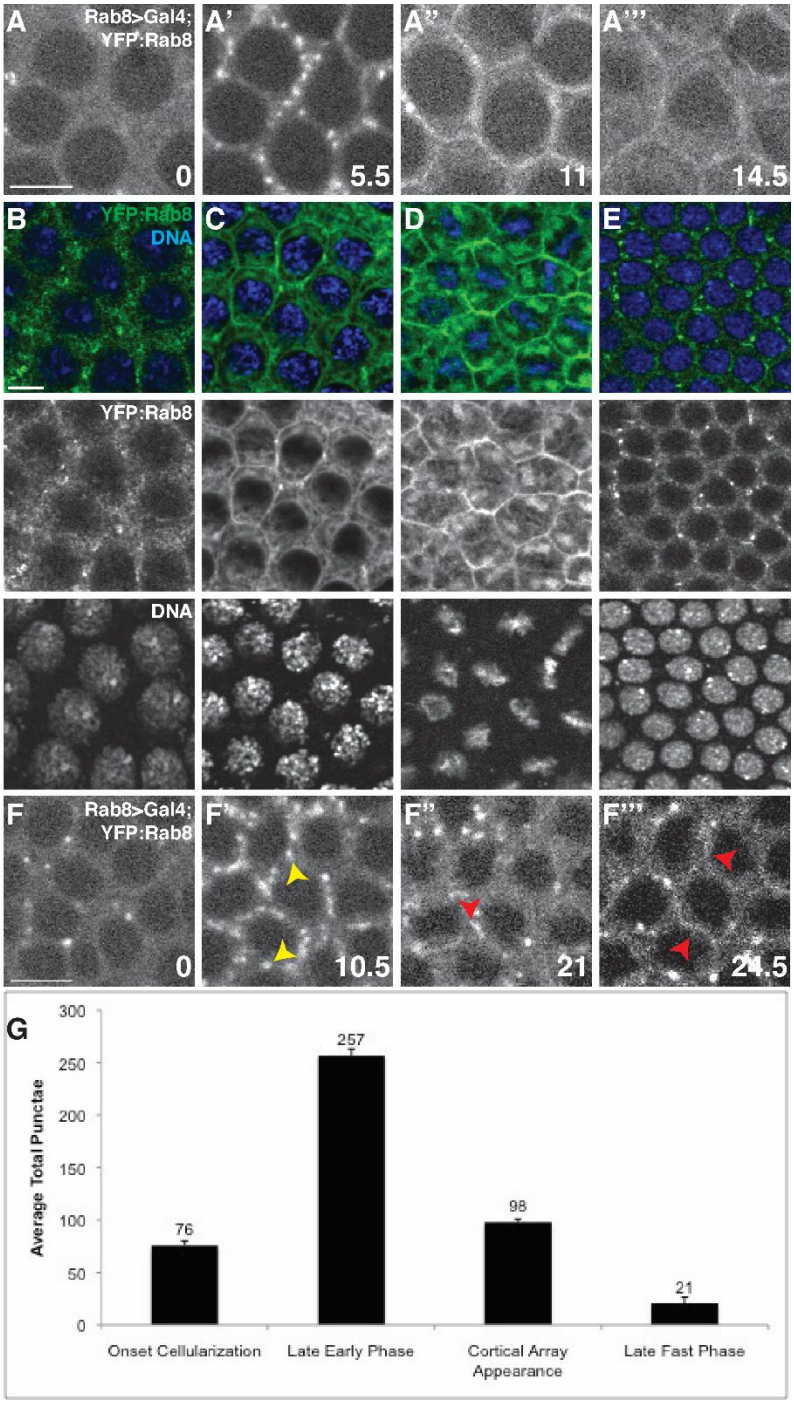

Figure 1. Rab8 exhibits dynamic behaviors associated with furrow ingression *in vivo*.
(A-A''') Still-frames at 0, 5.5, 11 and 14.5 min measured from the beginning of cycle 13 of a whole mount embryo expressing UASp-YFP:Rab8 driven by Rab8>Gal4 imaged in an apicolateral plane. Dark circular

regions are nuclei. (A) At early cycle 13, Rab8 exists in punctate populations. (A') As the cycle proceeds, these puncta become more numerous. (A") Rab8 begins to transition into a continuous, peripheral array and the cytoplasmic puncta become depleted. (A''') The peripheral array persists for the remainder of the division cycle. (B-E) Syncytial, fixed embryos expressing YFP:Rab8 and stained for anti-YFP (green) and DNA (Hoescht, blue) to indicate mitotic stage. (B) During interphase Rab8 exists in punctate structures. (C) Early in mitosis, Rab8 transitions to a plasma membrane-associated population. (D) This population remains present during metaphase and anaphase stages. (E) Rab8 returns to a punctate distribution at the onset of the next syncytial cycle. (F-F''') Still-frames at 0, 10.5, 21 and 24.5 min measured from the onset of interphase 14 of the same embryo shown in (A). (F) Rab8 exists in punctate structures at the onset of cellularization. (F') These puncta become more numerous as cellularization proceeds (yellow arrowheads). (F") At mid-cellularization, Rab8 begins to transition to a peripheral association (red arrowheads) and the cytoplasmic puncta become depleted. (F''') The peripheral array persists through the remainder of cellularization (red arrowheads). (G) Quantification of average total puncta during cellularization, including s.e.m. Scale bars in A,F are 10 µm; scale bar in B is 5 µm.

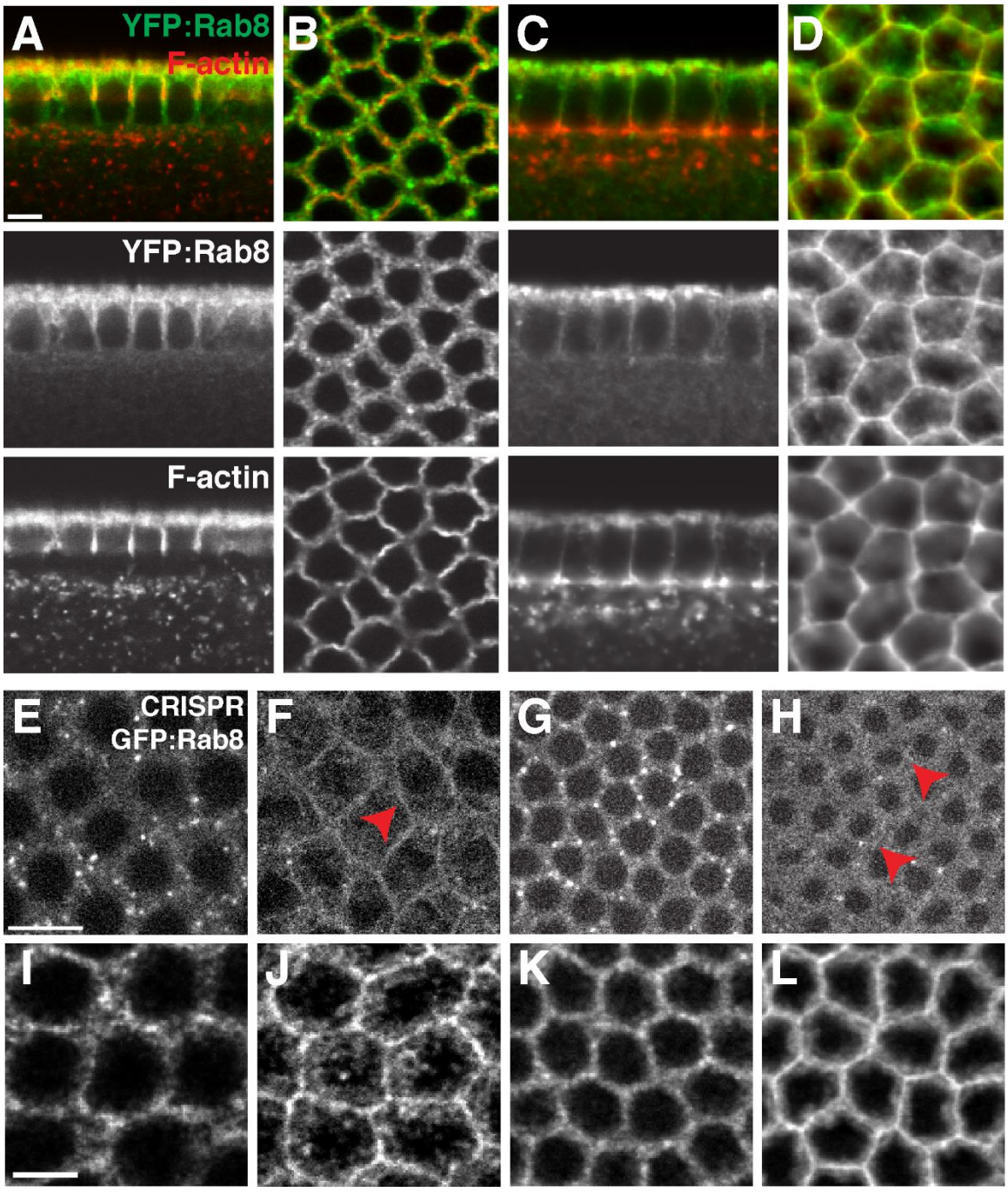

Figure 2. Rab8 transitions to the plasma membrane during the fast phase of cellularization.

(A-D) Localization of YFP:Rab8 (green) and F-actin (phalloidin, red) in fixed, cellularizing embryos. (A,B) During early cellularization, Rab8 exists in apical punctate populations (A, viewed along apical-basal axis; B, planar view of the same embryo). (C,D) As fast phase begins, Rab8 remains apically associated (C, apical-basal view) and transitions to a peripheral population (D, planar view of the same embryo imaged in

an apicolateral plane just above the level of the nuclei). (E-H) Live imaging stills of embryos expressing CRISPR GFP:Rab8 shows transition from puncta (E,G) to peripheral array (F,H; red arrowheads) in syncytial (E,F) and cellularization (G,H) stages. (I-L) Fixed images of embryos expressing CRISPR GFP:Rab8 (anti-GFP) show same transitions in syncytial (I,J) and cellularization (K,L) stages. Scale bar in A is 5 µm; scale bars in E,I are 10 µm.

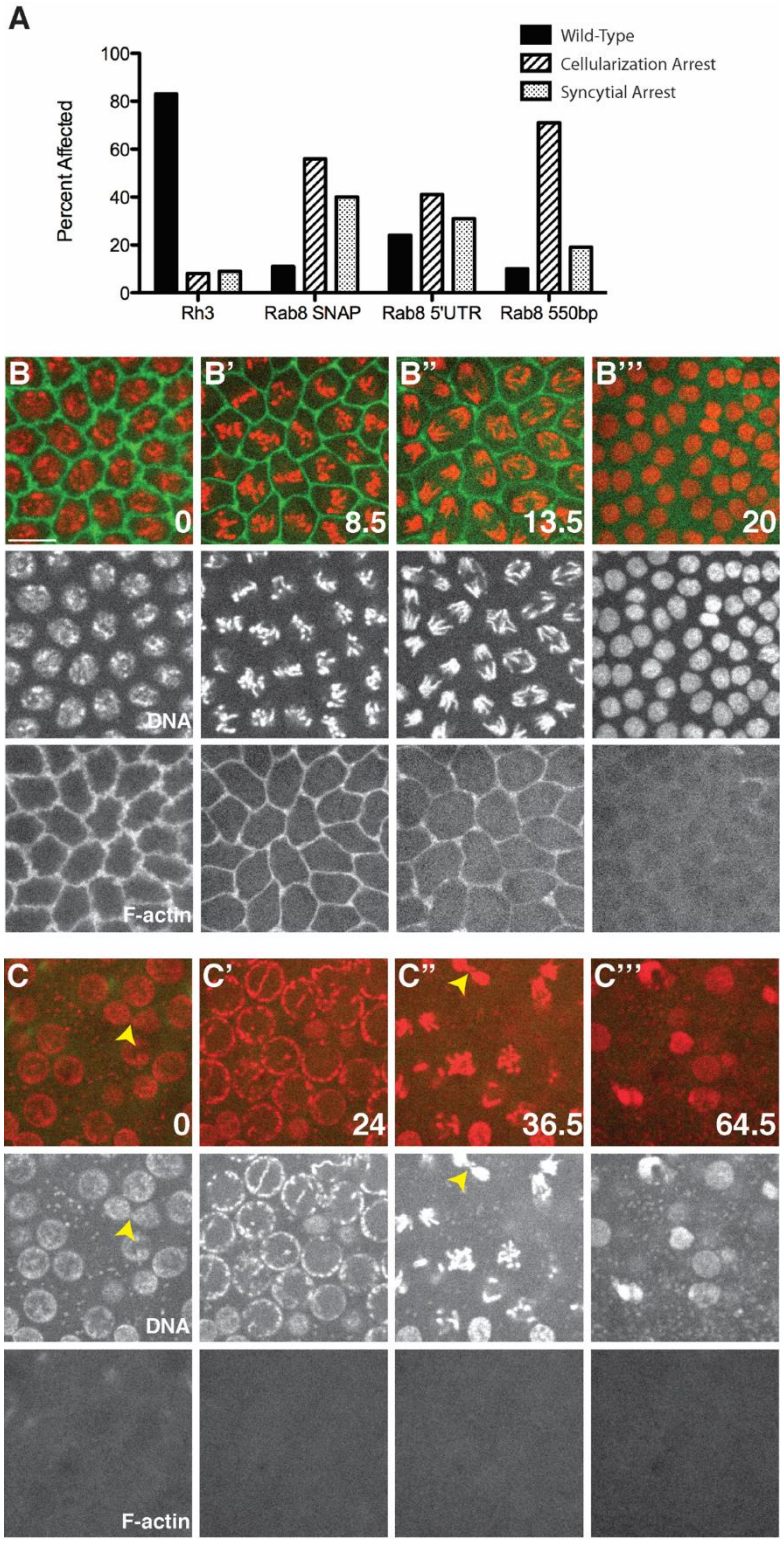

Figure 3. Knockdown of Rab8 severely disrupts furrow ingression in the early embryo.

(A) Embryos were injected with control or Rab8 dsRNA prepared against two different regions of Rab8 and phenotypic defects were quantified. Control Rh3 dsRNA (n=87), Rab8 SNAP (n=89), Rab8 5'UTR (n=70), Rab8 550bp (n=21). $p < 0.0001$ for all changes in proportions across groups. $p < 0.0001$ for each treatment group when compared to proportions seen in control dsRNA injected embryos. (B-C) Embryo expressing Histone:RFP (marking chromosomes, red) and GFP:MoeABD (marking F-actin, green). (B-B''') Still-frames of Rh3 dsRNA control-injected embryo at 0, 8, 13.5 and 20 min imaged from a planar orientation. (B) Control embryos show proper ingression of F-actin furrows during the mitotic division cycle. (B' and B") F-actin furrows have ingressed to the level of the nuclei during DNA condensation (B') and metaphase alignment (B''). (B''') Post-division, F-actin furrows regress back to the apical surface. (C-C''') Still frames of Rab8 RNAi injected embryos at 0, 24, 36.5 and 64.5 min imaged in a planar orientation. (C) F-actin furrows fail to form and result in a failure of nuclear divisions (yellow arrowhead). (C'-C''') F-actin furrows are absent and nuclei show irregular spacing and failure of proper separation (C", arrowhead). Aberrant nuclei undergo nuclear fallout and lose attachment, depleting the cortical nuclear layer (C", C'''). Scale bar is 10 µm.

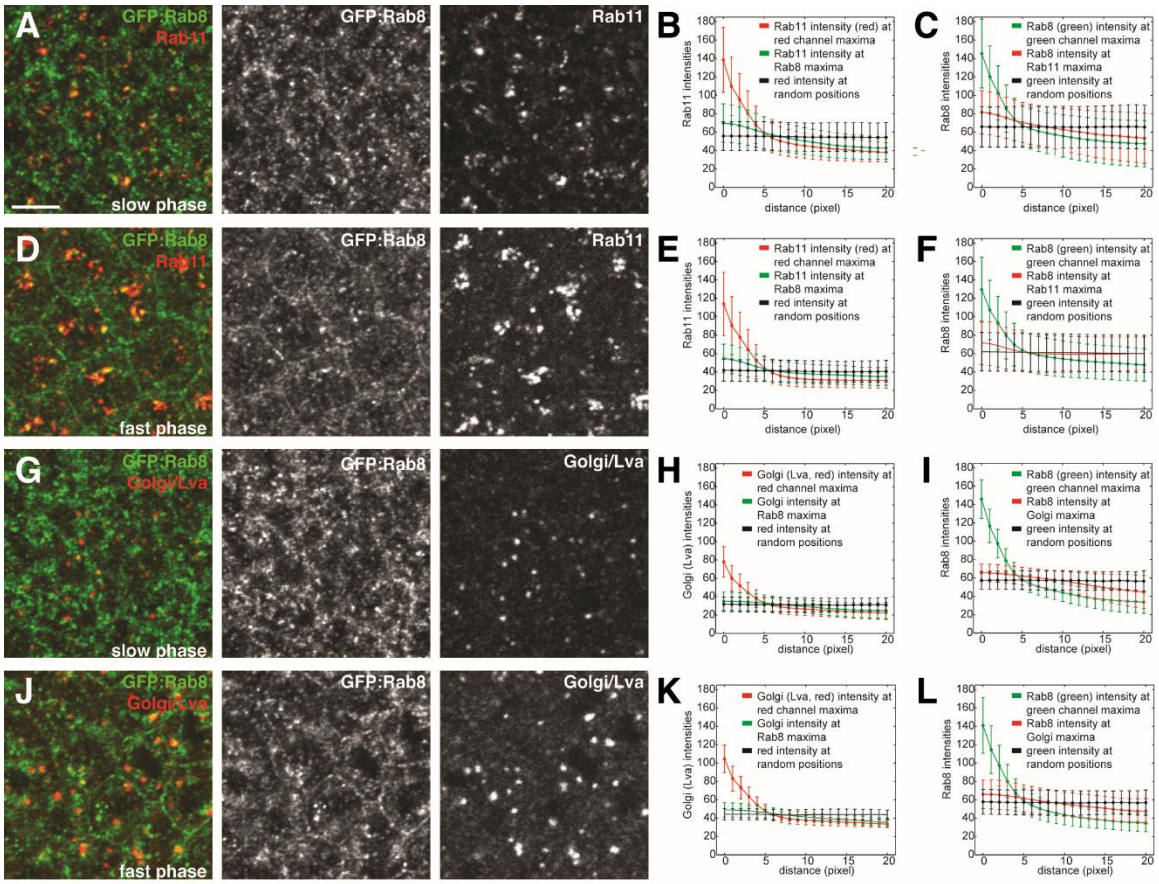

Figure 4. Rab8 displays partial coincidence with Rab11 and the Golgi.

(A-F) CRISPR GFP:Rab8 in green (anti-GFP); RE (anti-Rab11), in red. (A) Slow phase cellularization embryo. Rab8 puncta are largely distinct from the RE, however occasional overlap between compartments is seen. (B,C,E,F) Distance plots of Rab11 intensities (B,E) or Rab8 intensities (C,F) from indicated local maxima during slow phase (B,C) or fast phase (E,F) of cellularization. (D) During fast phase cellularization, Rab8 puncta become more enriched in subdomains of REs. (G-L) CRISPR GFP:Rab8 in green (anti-GFP); Golgi (anti-Lva), in red. (G) Slow phase cellularization embryo. Rab8 puncta are largely distinct from the Golgi with rare overlap between compartments. (H,I,K,L). Distance plots of Golgi intensities (H,K) or Rab8 intensities (I,L) from indicated local maxima during slow phase (H,I) or fast phase (K,L) of cellularization. (J) During fast phase cellularization, Rab8 puncta become more enriched at the Golgi. $p < 0.05$ for Rab11 and Lva intensity at Rab8 maxima during late cellularization (E,K). $p < 0.15$ for Rab11 intensity at Rab8 maxima during early cellularization (B), and for Rab8 intensity at Rab11 maxima during early cellularization (C). Scale bars are 5 µm.

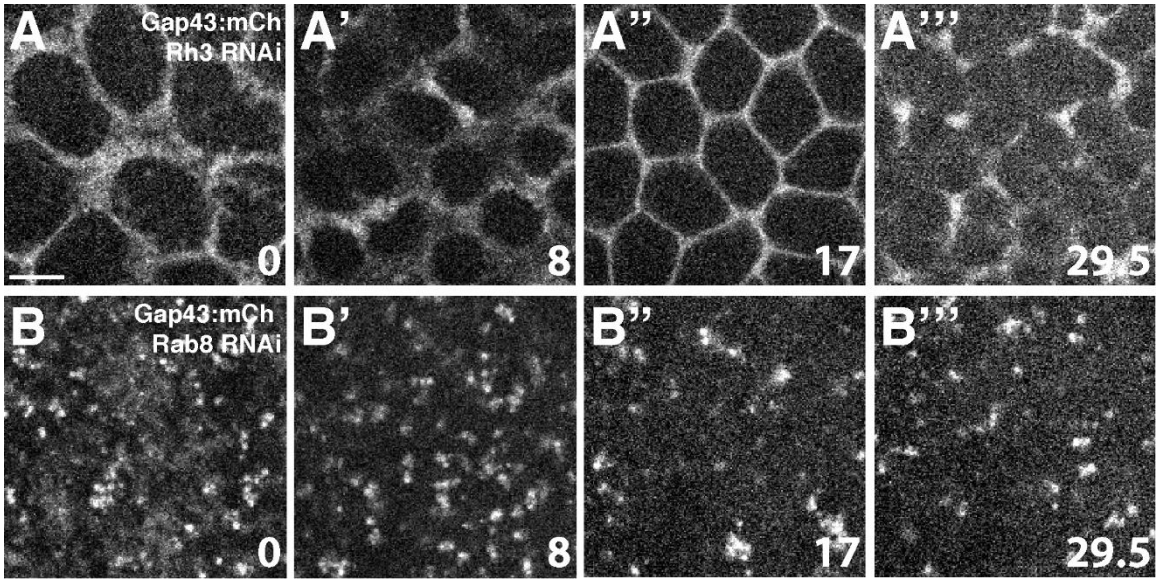

Figure 5. Rab8 is required to deliver plasma membrane components to the cell surface during furrow formation.

(A-A''') Control dsRNA-injected control embryo expressing Gap43:mCherry at 0, 8, 17 and 29.5 min. Gap43 associates with the plasma membrane and furrows during syncytial divisions. (B-B''') Rab8 RNAi treated embryo expressing Gap43:mCherry at 0, 8, 17 and 29.5 min. Knockdown of Rab8 results in Gap43 existing in cytoplasmic puncta and a failure of trafficking to the cell surface. Scale bar is 10 μm.

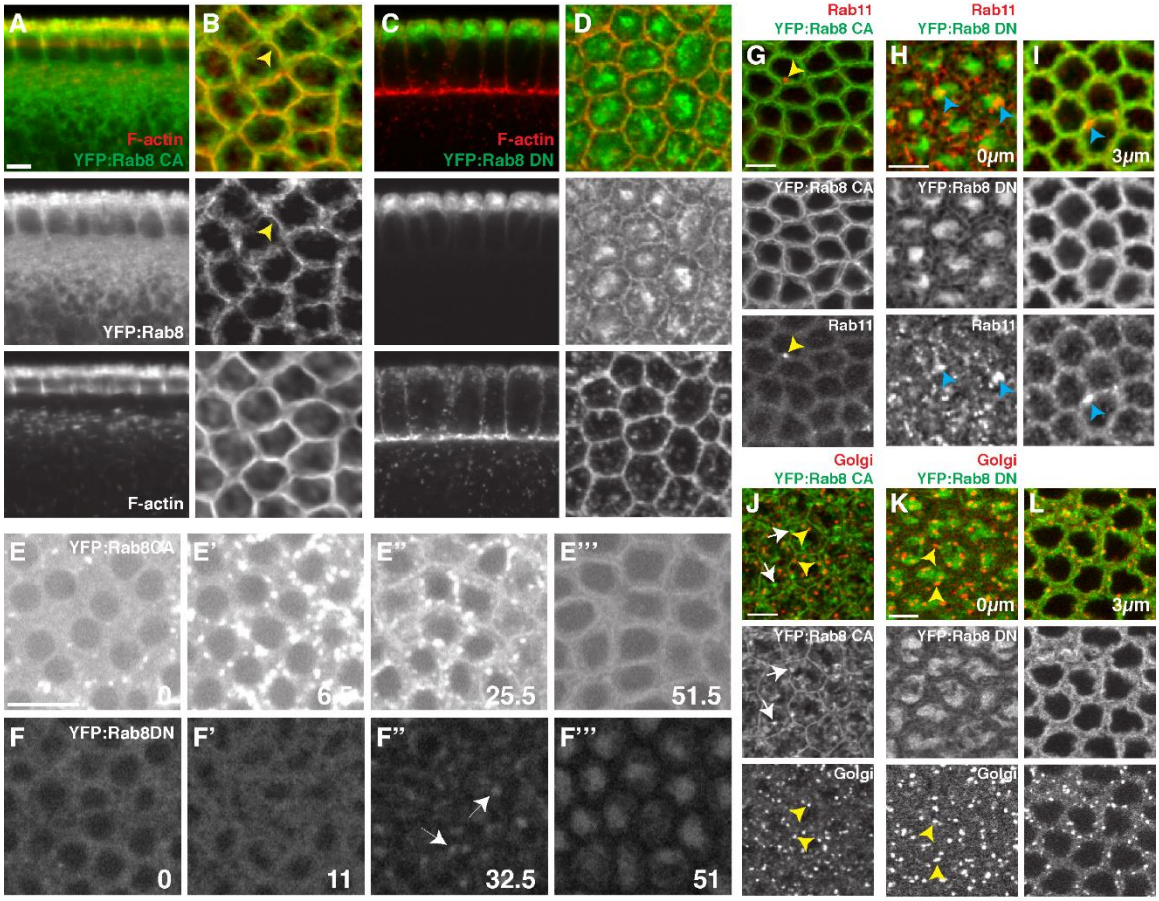

Figure 6. Rab8 punctate and plasma membrane-associated behaviors are GTPase activity dependent *in vivo*.

(A,B) YFP:Rab8 CA (GTPase deficient) in green (anti-GFP); F-actin, (phalloidin) in red. Fixed images show that Rab8 CA localizes apically in early cellularization stages (A, apical-basal view) and prematurely forms a peripheral array (B, arrowhead, planar view of the same embryo). (C,D) YFP:Rab8 DN (GDP-dissociation deficient) in green (anti-GFP); F-actin, phalloidin, in red. Large aggregates of Rab8 DN form above the nuclei in the cytoplasm (C, apical-basal view; D, planar view, same embryo). (E-E''') Still-frames of live-imaged, intact YFP:Rab8 CA embryo at 0, 6.5, 25.5 and 51.5 min measured from the onset of interphase 14. (E) Initially, Rab8 CA exists in punctate structures. (E') These puncta become more numerous, and then Rab8 CA transitions to a peripheral array (E''). (E''') The association with the plasma membrane persists through cellularization. (F-F''') Still-frames of live-imaged, intact YFP:Rab8 DN embryo at 0, 11, 32.5 and 51 min measured from the onset of interphase 14. (F, F') Punctate structures are lacking in Rab8 DN embryo at the onset (F) and early (F') stages of cellularization. (F'') As cellularization proceeds, cytoplasmic aggregates begin to form (arrowheads). (F''') In later stages, aggregates become larger and denser. Imaging conditions are identical between (E) and (F) for comparison. (G-I) YFP:Rab8 CA or DN in green (anti-GFP); RE (anti-Rab11), in red. (G) Rab8 CA peripheral array is distinct from RE compartments (yellow arrowhead) and Rab8 puncta are largely absent from the cytoplasm. (H) Rab8 DN

forms large aggregates at the apical surface; these aggregates remain largely distinct from RE puncta (blue arrowheads); however, the RE is enlarged in Rab8 DN expression (blue arrowheads). (I) At more basal levels (3µm below H) Rab8 DN is largely cytoplasmic and RE compartments are enlarged (blue arrowheads). (J-L) YFP:Rab8 CA or DN in green (anti-GFP); Golgi (anti-Lva), in red. (J) Rab8 CA (arrows) and Golgi compartments (yellow arrowheads) also form separate populations and show little overlap at the onset of cellularization. (K,L) Rab8 DN aggregates do not colocalize with the Golgi (arrowheads); Rab8 DN expression does not cause an enlargement of the Golgi compartment at apical (K, 0µm) or more basal levels (L, 3µm from G). Scale bars in A,G,H,J,K are 5 µm. Scale bar in E is 10 µm.

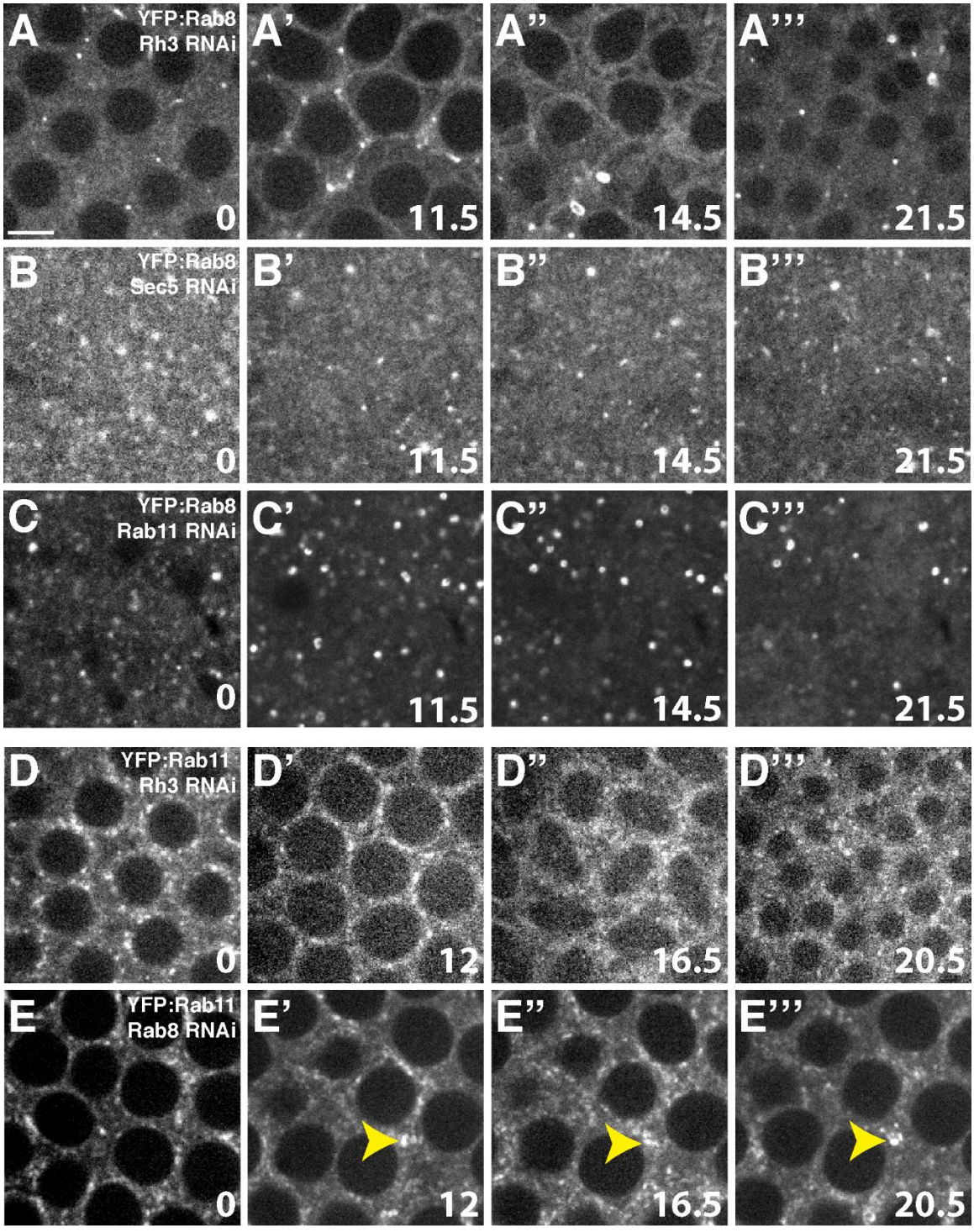

Figure 7. Rab8 requires the exocyst and RE function to behave dynamically and regulate membrane addition during furrow formation.

(A-A''') Control dsRNA-injected embryo expressing YFP:Rab8 at 0, 11.5, 14.5 and 21.5 min. Rab8 shows a transition from punctate to peripheral association over time. (B-B''') Sec5 RNAi treated embryo

expressing YFP:Rab8 at 0, 11.5, 14.5 and 21.5 min. Disruption of Sec5 results in a failure for Rab8 to adopt a peripheral localization over time. (C-C’’’) Rab11 RNAi treated embryo expressing YFP:Rab8 at 0, 11.5, 14.5 and 21.5 min. Disruption of the RE also results in a failure of Rab8 to localize peripherally. (D-D’’’) Control dsRNA-injected embryo expressing YFP:Rab11 at 0, 12, 16.5 and 20.5 min. Rab11 exists in punctate population over time during syncytial division cycles. (E-E’’’) Rab8 RNAi treated embryo expressing YFP:Rab11 at 0, 12, 16.5 and 20.5 min. Disruption of Rab8 does not appear to affect Rab11 population dynamics. Rab11 puncta appear slightly enlarged over time (arrowhead, E” and E’’’). All embryos imaged during syncytial furrow formation (cycle 12). Scale bar is 10 μm.

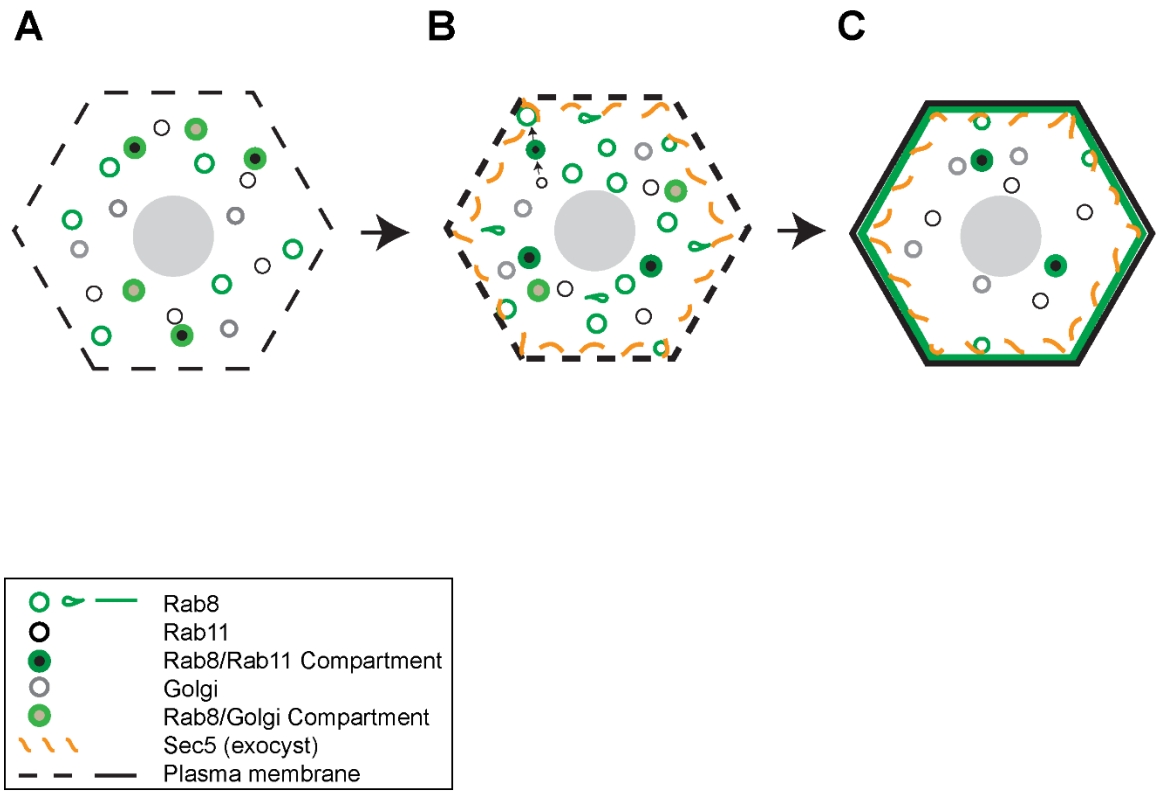

Figure 8. Rab8 regulates membrane addition and furrow formation during cellularization in a pathway that includes the recycling endosome and exocyst complex.

(A) Prior to the onset of cellularization, Rab8 is largely punctate in structure. (B) During the slow phase of furrow ingression, Rab8 puncta become more numerous and display partial colocalization with Golgi and Rab11 compartments. (C) By the fast phase of cellularization, Rab8 transitions to a peripheral association where it localizes with the exocyst (Sec5) and plasma membrane. Membrane delivery to the furrow occurs, where Rab8 may function to link RE and Golgi stores to the plasma membrane (arrows, B).

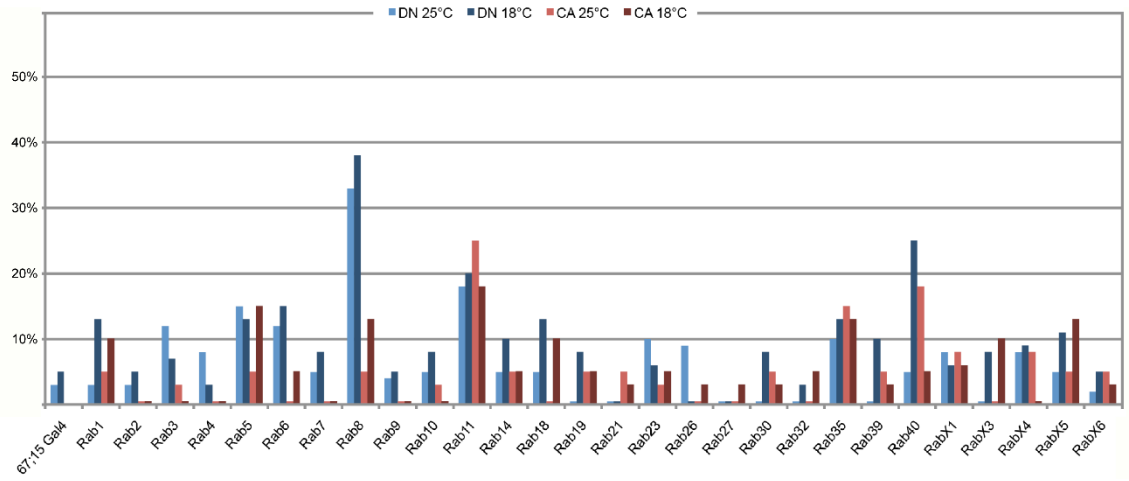

Figure S1. A screen of the effects of dominant-negative and constitutively-active Rab protein expression in the early *Drosophila* embryo.

Embryos from females expressing dominant-negative or constitutively-active Rab transgenes under the control of a maternal Gal4 driver line (matαTub-Gal4VP16 67C;15) were scored for gross tissue level developmental defects by transillumination under Halocarbon oil. Dominant-negative and constitutively-active Rab protein expression had only partially penetrant effects, consistent with partial Rab disruption when endogenous proteins are present. However, dominant-negative Rab8 expression produced the strongest disruption of early morphogenesis among the Rab proteins screened, with defects apparent during cellularization. n≥40 embryos for each condition tested (temperature and transgenic line).

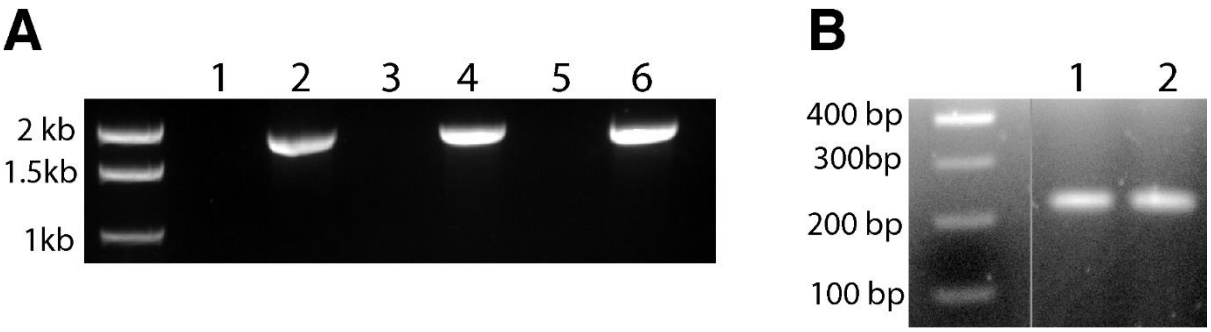

Figure S2. Successful CRISPR-mediated insertion of GFP into the *Drosophila Rab8* genomic locus.
(A) PCR verification of GFP:Rab8 insertion into the Rab8 genomic locus. Three primers pairs (lanes 1 and 2, 3 and 4, or 5 and 6) were designed with the 5' primer binding in the chromosomal DNA upstream of the cloned 1.5kb 5' donor homology arm. 3' primers were designed to bind to the GFP coding sequence. Successful amplification of these regions is only observed in CRISPR GFP:Rab8 embryos (lanes 2, 4 and 6), but not OreR control embryos (lanes 1, 3 and 5), demonstrating that GFP is properly inserted at the genomic Rab8 locus creating an N-terminal GFP fusion. (B) Control PCR against primers located in the Rab35 gene locus demonstrate DNA loading control of OreR control (lane 1) and CRISPR GFP:Rab8 (lane 2) genomic DNA products. Scale bar in A is 10µm; scale bar in E is 5µm.

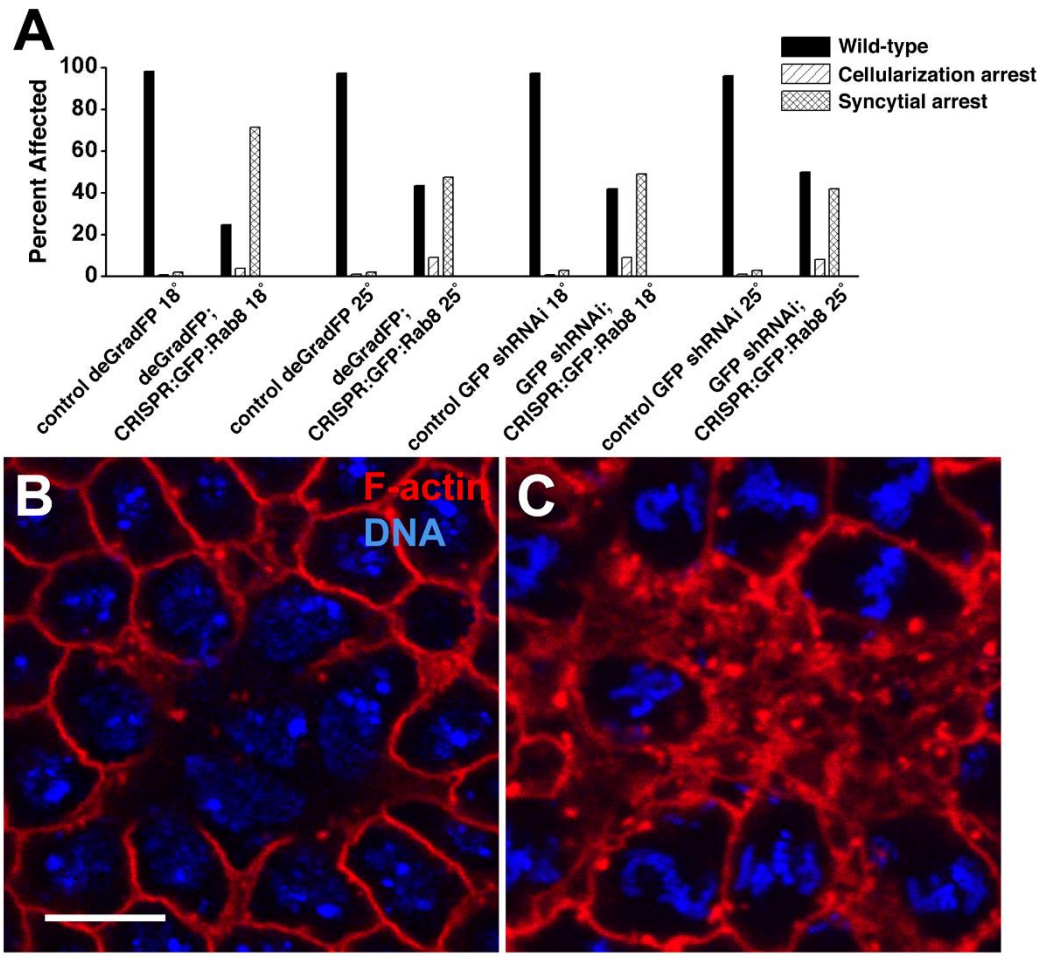

Figure S3. Disruption of Rab8 function by deGradFP and GFP TRiP shRNAi results in defects in early development and furrow formation.
(A) The development of homozygous CRISPR GFP:Rab8 embryos expressing either deGradGFP or GFP TRiP shRNAi was scored under oil for defects in early embryogenesis. Control embryos expressed either deGradGFP or GFP TRiP shRNAi in the absence of GFP:Rab8. $p < 0.001$ for all changes in proportions across groups. $p < 0.001$ for each treatment group when compared to proportions seen in control deGradFP or GFP shRNAi expressing embryos. (B,C) Embryos from either deGradFP; CRISPR GFP:Rab8 (B) or GFP TRiP shRNAi; CRISPR GFP:Rab8 (C) were fixed and stained for F-actin (phalloidin, red) or DNA (DAPI, blue). Local areas showing defects in furrow formation and ingression are shown in (B,C). Scale bar is 5µm.

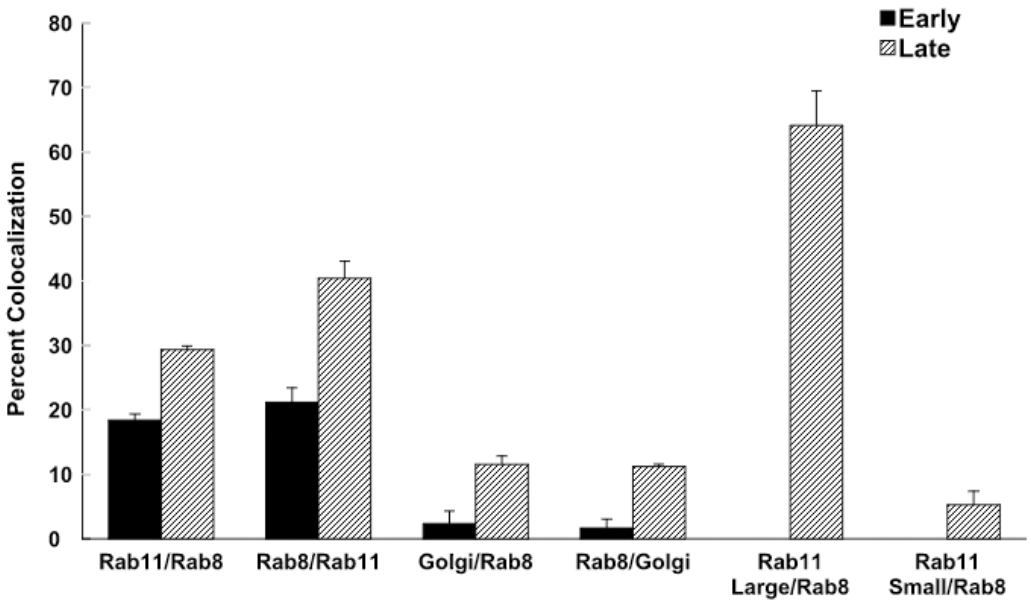

Figure S4. Analysis of Rab8 colocalization by compartment.
Measurement of colocalization frequencies by individual compartments. CRISPR GFP:Rab8 embryos were immunostained for Rab8 (anti-GFP), RE (anti-Rab11) or Golgi (Lva) and colocalization between compartments counted during slow or fast phase of cellularization. Error bars are standard deviation.

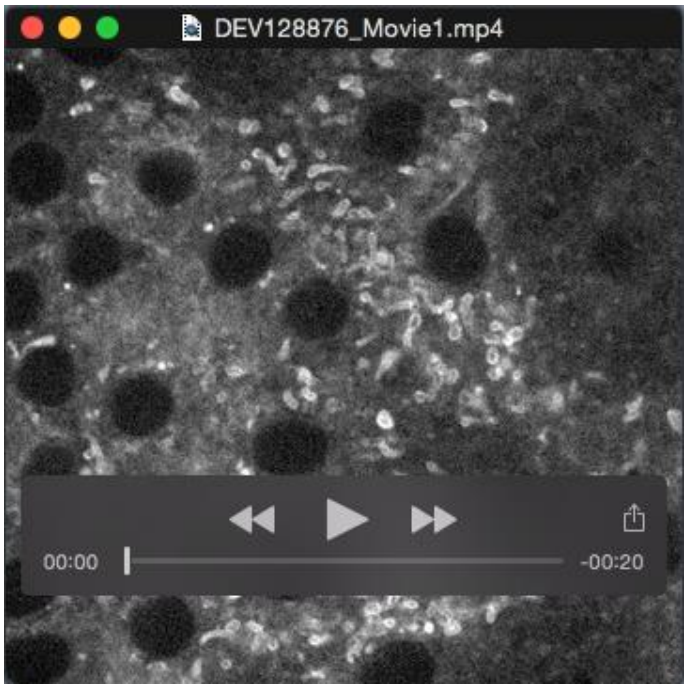

Movie 1. YFP:Rab8 localization prior to cycle 10 and the onset of furrow ingression. Rab8>Gal4 driven expression of UAS-YFP:Rab8 shows Rab8 present in large cytoplasmic compartments. Images acquired every 5 seconds.

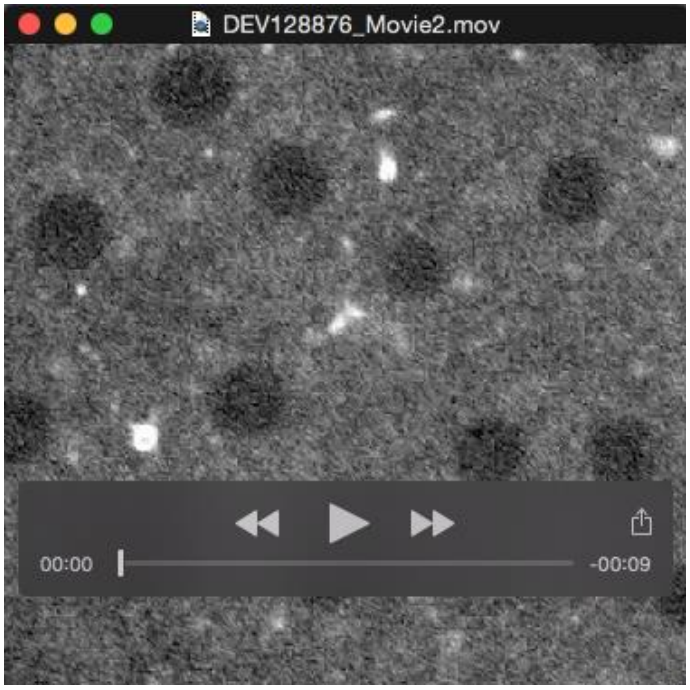

Movie 2. YFP:Rab8 localization during cycles 11 and 12 and the formation of syncytial furrows. Rab8>Gal4 driven expression of UAS-YFP:Rab8 shows Rab8 present in puncta that then become depleted as Rab8 transitions to an association with the plasma membrane. Images acquired every 30 seconds.

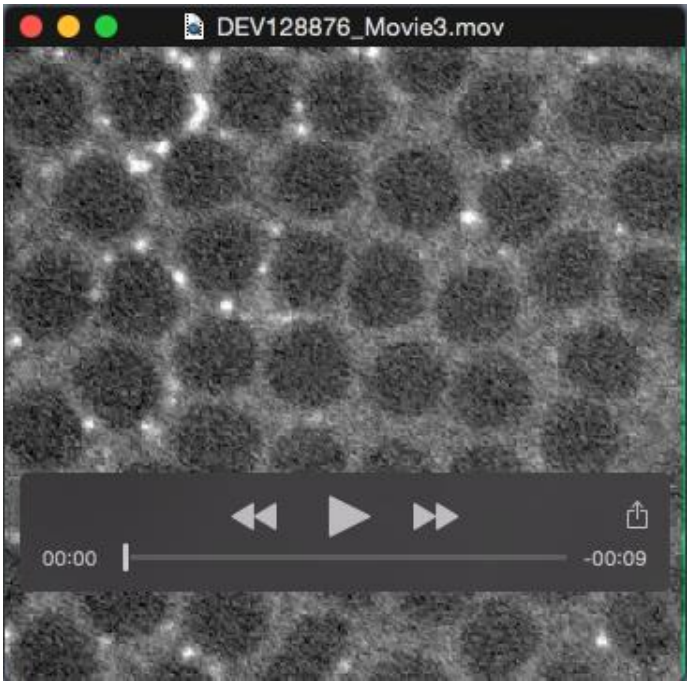

Movie 3. YFP:Rab8 localization during cycle 14 and cellularization. Rab8>Gal4 driven expression of UAS-YFP:Rab8 shows Rab8 present in puncta that then become depleted as Rab8 transitions to an association with the plasma membrane. Images acquired every 30 seconds.

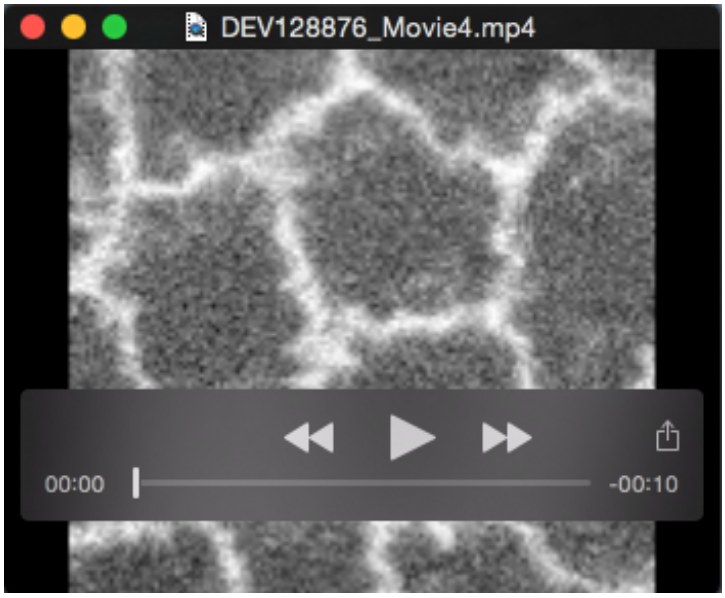

Movie 4. Control Rh3 dsRNA injected embryo expressing Gap43:mCh during syncytial furrow formation. Images acquired every 30 seconds.

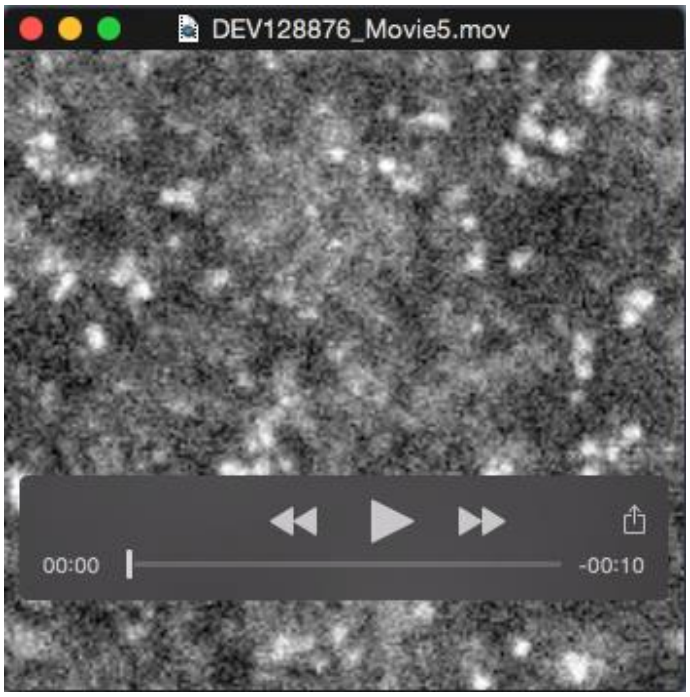

Movie 5. Rab8 dsRNA injected embryo expressing Gap43:mCh during syncytial furrow formation. Gap43:mCh accumulates in cytoplasmic compartments and fails to localize to the plasma membrane. Images acquired every 30 seconds.

Table S1. gRNAs and primers

Name	Sequence
gRNAs for CRISPR GFP:Rab8	
5′chiRNA-1	CTTCGAACAGATAGTCGTAGGTTT
3′chiRNA-1	AAACAAACCTACGACTATCTGTTC
5′chiRNA-2	CTTCGCCCGATAATAGTGCTTAGC
3′chiRNA-2	AAACGCTAACGACTATTATCGGGC
Cloning primers for HDR donor GFP:Rab8	
5′CRISPRRab8(1)SpeI	GGACTAGTAAAATGCTCCCCTTTCATTAT
3′CRISPRRab8(1)BamHI	CGGGATCCTTTGTGTGCTTTTGCGGTAG
5′CRISPRGFPBamHI	CGGGATCCGTTGTACAGCTCGTCCATGC
3′CRISPRGFPSalI	ACGCGTCGACCGCCCCGCCCTGCCACTCAT
5′CRISPRRab8(2)SalI	ACGCGTCGACATGGCCAAAACCTACGACTA
3′CRISPRRab8(2)KpnI	GGGGTACCTATATAAATAAAATGTTTGT
Primers for PCR verification of CRISPR GFP:Rab8 insertion	
5′PCR-1	TGACATGCAGAATTAAAAGCCC
3′PCR-1	CGGACACGCTGAACTTGTG
5′PCR-2	ATGACATGCAGAATTAAAAGCCCA
3′PCR-2	GTCAGCTTGCCGTAGGTGG
5′PCR-3	TGACATGCAGAATTAAAAGCCCAAT
3′PCR-3	GCTGAACTTGTGGCCGTTTAC